Climate Dynamics (2024) 62:10503–10523
https://doi.org/10.1007/s00382-024-07453-2

ORIGINAL ARTICLE

Greenland summer blocking characteristics: an evaluation of a high-resolution multi-model ensemble

Linh N. Luu[1] · Edward Hanna[1] · Dilkushi de Alwis Pitts[1,4] · Jacob Maddison[2] · James A. Screen[2] · Jennifer L. Catto[2] · Xavier Fettweis[3]

Received: 4 March 2024 / Accepted: 20 September 2024 / Published online: 16 October 2024

Abstract
Atmospheric blocking is a phenomenon that can lead to extreme weather events over a large region, yet its causes are not fully understood. Global climate models show limitations in representing Northern Hemisphere blocking, especially its frequency, and decadal variability in Greenland blocking in summer in the recent decades. In this study we evaluate the ability of high-resolution (HighResMIP) Earth System Models (ESMs) to simulate summer blocking over the Greenland area, using different but complementary methods to describe the characteristics of blocking. We find that the HighResMIP ensemble can reproduce the spatial pattern of Greenland blocking events, albeit with systematic biases, and capture the relative frequencies of the main blocking patterns: namely the wave breaking structure, North Atlantic ridge, and omega-type blocking. However, the HighResMIP ensemble fails to simulate the observed temporal variations of Greenland blocking index (GB2) and the extremely high values of daily GB2 observed in recent decades. In addition, we do not find clearly superior representation of blocking features from higher-resolution in HighResMIP models compared with lower-resolution models. We also find large sea surface temperature (SST) biases over the North Atlantic and seas surrounding Greenland, and biases in moisture transport over the North Atlantic toward Greenland, especially over the western flank of blocking areas, which might together contribute to model biases in the representation of blocking magnitude.

Keywords Blocking · Greenland · Atmospheric Dynamics · Weather Regimes · Climate Models

1 Introduction

Atmospheric blocking (stationary or slow-moving high-pressure systems) has been acknowledged as a prominent large-scale atmospheric feature for over a century and was formally documented by a term 'blocking action' in Elliott and Smith (1949). Following this, blocking was investigated descriptively and statistically in Rex (1950b, a), respectively, while blocking definitions, causes and impacts have received great attention and debate from the scientific community since then (Liu 1994). In general terms, a block is a large-scale (typically several hundred km wide), strong and persistent (a few days to several weeks or occasionally longer-lasting) anticyclonic system in the troposphere that interrupts and deflects zonal flows in midlatitude regions (Barrett et al. 2020; Nakamura and Huang 2018; Pasquier et al. 2019; Pettersen et al. 2022), although it also occurs at higher latitudes such as Greenland (e.g., Hanna et al. 2016). Blocking occurs with different circulation patterns including: (i) a Rossby wave-breaking pattern where a ridge is extended and folded over a cyclonic system in a dipole structure with an anticyclonic anomaly on the poleward side of a cyclonic anomaly, (ii) a stationary amplified ridge that develops and advects warm air from the subtropics into the mid latitude regions, and (iii) omega blocking that is similar to (ii) but the amplitude of the anticyclone is intensified and it is bounded by upstream and downstream cyclonic systems with which it forms an omega-shaped pattern of flow (Woollings et al. 2018; Kautz et al. 2022). Over the Greenland region, these

✉ Linh N. Luu
lluu@lincoln.ac.uk

1 Department of Geography, University of Lincoln, Lincoln, UK

2 Department of Mathematics and Statistics, University of Exeter, Exeter, UK

3 Department of Geography, University of Liège, Liège, Belgium

4 College of Interdisciplinary Studies, Zayed University, Dubai, UAE

three patterns also happen alternately and may transform into one another over periods of a few days (Preece et al. 2022; Michel et al. 2012).

Greenland blocking (GB) is observed to be more persistent than blockings over other areas, e.g., European blockings and low-latitude blocking over the Atlantic (Davini et al. 2012), and has large impacts on regional weather as well as the Northern Hemisphere climate system (Hanna et al. 2016). Many studies have pointed out that extreme summer warmth over Greenland associated with GB episodes in the last 10–15 years has led to massive icesheet melting in the region and thus contributed to global sea-level rise (Preece et al. 2022; Ballinger et al. 2019; Fettweis et al. 2013; Nghiem et al. 2012; Hanna et al. 2021; Mcleod and Mote 2015). In addition, Wang et al. (2019) shows that increased GB in summer is likely to contribute to surface warming over northern Canada and eastern Siberia due to the increase in downward infrared radiation associated with enhanced moisture flux convergence over those regions during GB episodes. These summer GB episodes are also associated with enhanced summer precipitation over the northeastern US (Simonson et al. 2022) and the UK (Hanna et al. 2017). Additionally, winter GB episodes are linked with a positive mean precipitation anomaly (Yao and De-Hai 2014) and an increase in the chance of extreme precipitation over southern Europe (Lenggenhager and Martius 2019) and are often associated with cold and snowy weather across the British Isles (Greening and Hodgson 2019). Mattingly et al. (2015) show that strong GB episodes can deflect hurricanes moving northeastwards so that they curve back west and make landfall on the US northeastern coast, as occurred with Hurricane Sandy in October 2012.

Simulating and predicting atmospheric blocks has been a major challenge for several decades due to the complex nature of blocking and remaining deficiencies in the understanding of its initiation and evolution (Davini and D'andrea 2016). Climate models tend to underestimate blocking frequency and persistence over both the Euro-Atlantic and Pacific regions, although overall performance is somewhat improved in the latest generation of Earth System Models (ESM) in the Coupled Model Intercomparison Project phase 6 (CMIP6, Eyring et al. 2016), compared with CMIP5 and CMIP3 (Davini and D'andrea 2020; Schiemann et al. 2020). This recent improvement in the representation of blocking might be explained by an increase in model horizontal resolution leading to a better model representation of the mean state, orography, and eddy flux (Anstey et al. 2013; Davini et al. 2017; Berckmans et al. 2013). However, increasing model resolution does not consistently improve the performance of seasonal blocking frequency, and in particular there is a lingering bias for summer (Davini and D'andrea 2020; Schiemann et al. 2017). Jury et al. (2019) found that a high-resolution ensemble from un-nudged regional climate models (RCM) in EURO-CORDEX also underestimates the frequency of blocking, especially at the centre of the integration domain where the RCM dynamics are free from reanalysis boundary forcing information, when there is no spectral nudging into RCMs. However, model vertical resolution and lid height (i.e., the height of the top level of the model) could also play a role in how well blocking frequency is simulated (Anstey et al. 2013). Dawson and Palmer (2015) showed that global climate models (GCMs) can simulate quasi-persistent weather regimes, including atmospheric blocking, at very high horizontal resolution (roughly 16 km) that is normally used in short-to-medium range weather prediction. However, this approach is not yet realistic for long-term climate simulations due to its huge computational cost, although given the fast development of technologies and computing resources, it could relatively soon become possible. Dawson and Palmer (2015) also demonstrated that an improvement in representation of local-scale processes by stochastically perturbing total parametrized tendency of physical processes, rather than explicitly resolving them using higher-resolution approach, can computationally improve large-scale climate features in coarser resolution GCMs. Steinfeld and Pfahl (2019) found that diabatic heating upstream of the blocking has a significant impact on the onset, intensification, and persistence of blocking, depending on different blocking cases and regions. This suggests that improvements in the representation of the microphysics of cloud feedbacks and the coupling of dry and moist processes in climate models are crucial for blocking representation (Steinfeld et al. 2020; Maddison et al. 2020).

In this study, we use meteorological reanalysis data to investigate blocking characteristics including temporal trends and spatial patterns, with a focus on the Greenland region. We then statistically evaluate how well the global climate models in the HighResMIP ensemble (Haarsma et al. 2016) reproduce those blocking features over Greenland and

Table 1 Description of HighResMIP simulations used in this study

No	GCM	Horizontal resolutions		Number of Members
		Atmosphere	Ocean	
1	CNRM-CM6-1	2.5 degree	1 degree	1
2	CMCC-CM2-HR4	1 degree	0.25 degree	1
3	CMCC-CM2-VHR4	0.25 degree	0.25 degree	1
4	EC-Earth3P	1 degree	1 degree	3
5	EC-Earth3P-HR	0.5 degree	0.25 degree	3
6	ECMWF-IFS-HR	0.25 degree	0.25 degree	6
7	ECMWF-IFS-LR	0.5 degree	1 degree	8
8	ECMWF-IFS-MR	0.5 degree	0.25 degree	3
9	MPI-ESM1-2-HR	1 degree	0.5 degree	1
10	MPI-ESM1-2-XR	0.5 degree	0.5 degree	1

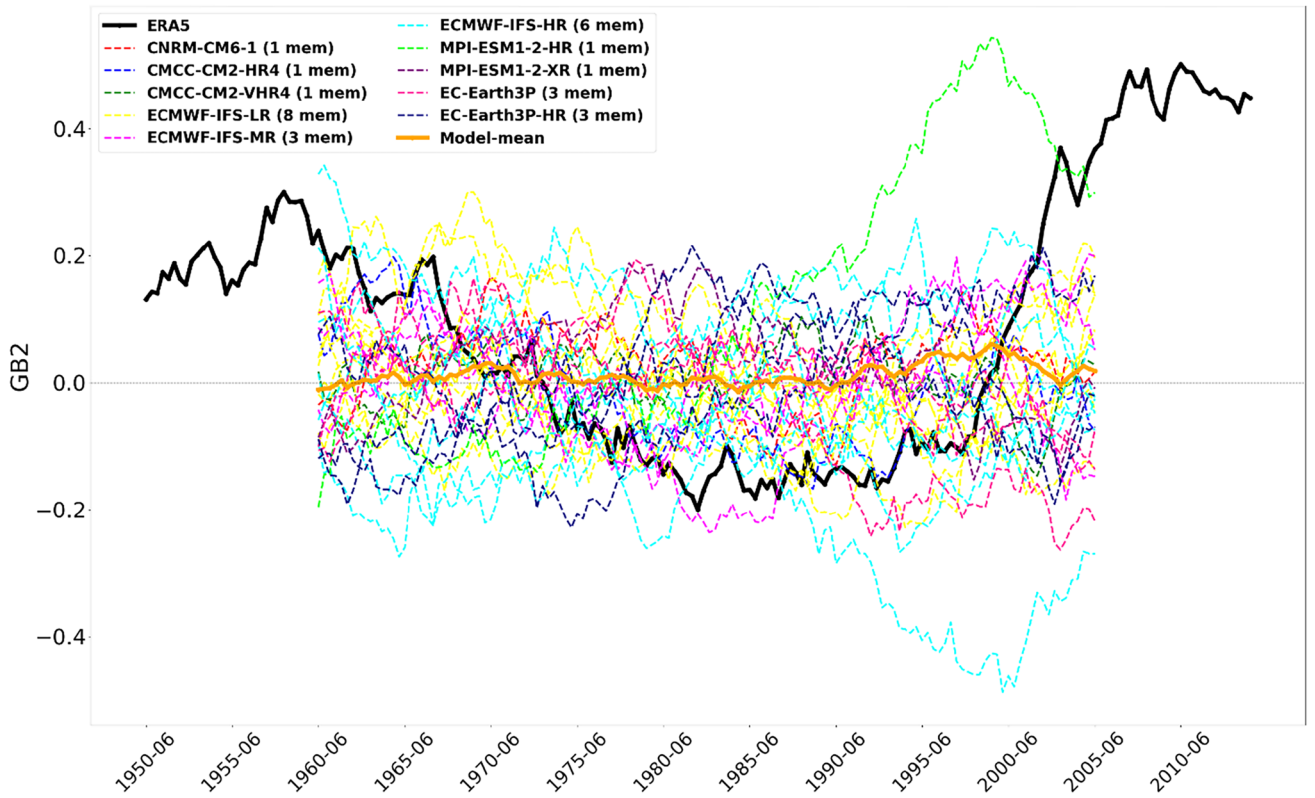

Fig. 1 20-year running mean time series of monthly GB2 in summer from ERA5 (1940–2023) and HighResMIP ensemble (1950–2014). All members from the same model have the same color and are plotted in thin dotted lines. The ERA5 and all model mean are plotted in black and orange thick solid lines, respectively

to what extent the results depend on model resolution. This paper is organised according to the following structure. The utilised climate data, blocking indices and Self Organising Maps methodology are described in Sect. 2, followed by the results and discussion in turn in Sect. 3, and finally some conclusions are drawn in Sect. 4.

2 Data and methods

2.1 Reanalysis and HighResMIP simulations

In this study, we use geopotential height at 500 hPa (z500) as a proxy for the large-scale circulation and to compute GB indices described in the next session. We extract daily mean z500 from the ECMWF's ERA5 reanalysis database (Hersbach et al. 2020). This dataset has a horizontal resolution of 0.25 degree and spans from 1940 to present. In addition, we use an ensemble from the HighResMIP simulations which are a higher-resolution version of CMIP6 in either the horizontal or vertical direction of each coupled component and share most forcing fields with other CMIP6 simulations (Haarsma et al. 2016). However, HighResMIP uses time-varying anthropogenic aerosol forcing from the MACv2.0-SP model, which is simplified to enhance the consistency of aerosol representation among models, as well as a fixed land-use and vegetation cover and does not include a dynamic vegetation model. Here, we use the HighResMIP Tier 2 simulations, which are coupled runs for the historical period spanning from 1950 to 2014. For each model, we explore at least one lower-resolution version, either atmosphere or ocean component, and one higher-resolution version, except the CNRCM-CM6-1 for which only a low resolution is available for z500. Relevant details of the HighResMIP models are provided in Table 1.

2.2 Greenland blocking indices.

Greenland Blocking Index (GBI) is a well-known index that depicts the area-weighted average of z500 covering the Greenland area from 80 to 20°W and 60–80°N (Hanna et al. 2016, 2018b). Here, we used a modified version of GBI, called GB2, for which we subtract the area-weighted daily average of z500 over the Northern Hemisphere band between 60 and 80°N. This mitigates the effect of thermodynamic changes due to anthropogenic greenhouse warming (and its seasonal cycle) over Greenland (Delhasse et al. 2021). We then normalize the index according to day of

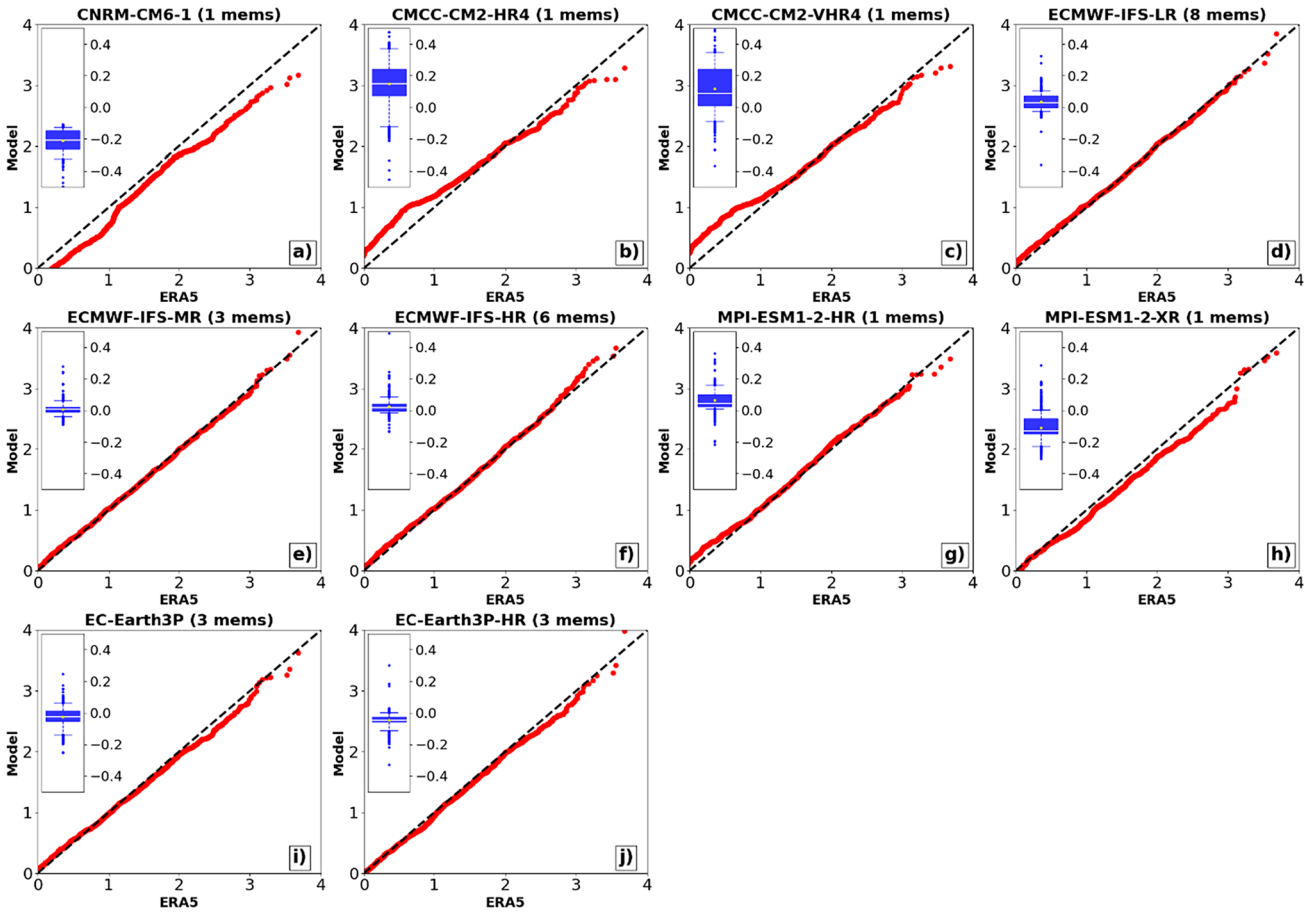

Fig. 2 Quantile–Quantile plot of GB2 values of all blocking days between ERA5 (1950–2014) and all HighResMIP models (1950–2014). All red points show GB2 values of corresponding quantiles in the distribution of models (ordinate) and ERA5 (abscissa). We consider all blocking events defined by criteria of either GB2 or D12 indices. All members from the same GCM are pooled together. The boxplot embedded within each panel shows the difference of quantiles on GB2 distribution between the model and ERA5. The box shows the interquartile range (25th–75th percentiles), the whiskers show a range of 5th to 95th percentiles, and those outliers are extreme points outside the whisker range. GB2 is a standardized, hence dimensionless index

year by subtracting the multi-year mean of the index over a baseline period of 1951–2000, the period just prior to strong Artic warming period as used in Hanna et al. (2022), and dividing the resulting values by their corresponding multi-year standard deviation to obtain the GB2 timeseries. We use this GB2 index to define blocking episodes using two criteria. First, we select all cases whose GB2 values exceed one standard deviation of the respective GB2 daily timeseries. Second, the first condition must span at least 4 consecutive days to emphasise the persistent aspect of blocking (Preece et al. 2022; Ward et al. 2020).

In addition to GB2 which only considers the magnitude of high-pressure over Greenland, we use another approach based on the reversal of the meridional gradient of geopotential height and air flow (Davini et al. 2012) to detect blocking events over Greenland (hereafter denoted as D12 index). This index considers both the spatial structure and propagation of high-pressure systems and can therefore be used to complement GB2. The index includes gradients computed from z500 to the north and south of each grid point over the region of interest, namely GHGN and GHGS, calculated using the following equations:

$$GHGN_{\lambda,\phi_0} = \frac{z500_{\lambda,\phi_N} - z500_{\lambda,\phi_0}}{\phi_N - \phi_0}$$

$$GHGS_{\lambda,\phi_0} = \frac{z500_{\lambda,\phi_0} - z500_{\lambda,\phi_S}}{\phi_0 - \phi_S}$$

where $\phi_N = \phi_0 + 15$ and $\phi_S = \phi_0 - 15$. λ, ϕ_0 are longitude and latitude, respectively. To identify instantaneous blocking at each grid point, we adopt the following conditions including: (i) GHGN is less than – 10gpm; (ii) GHGS is greater than 0 gpm; and (iii) the z500 anomaly at that grid point is positive, where iii) demonstrates a ridging anomaly and avoids the situation where (i) and (ii) occur due to a

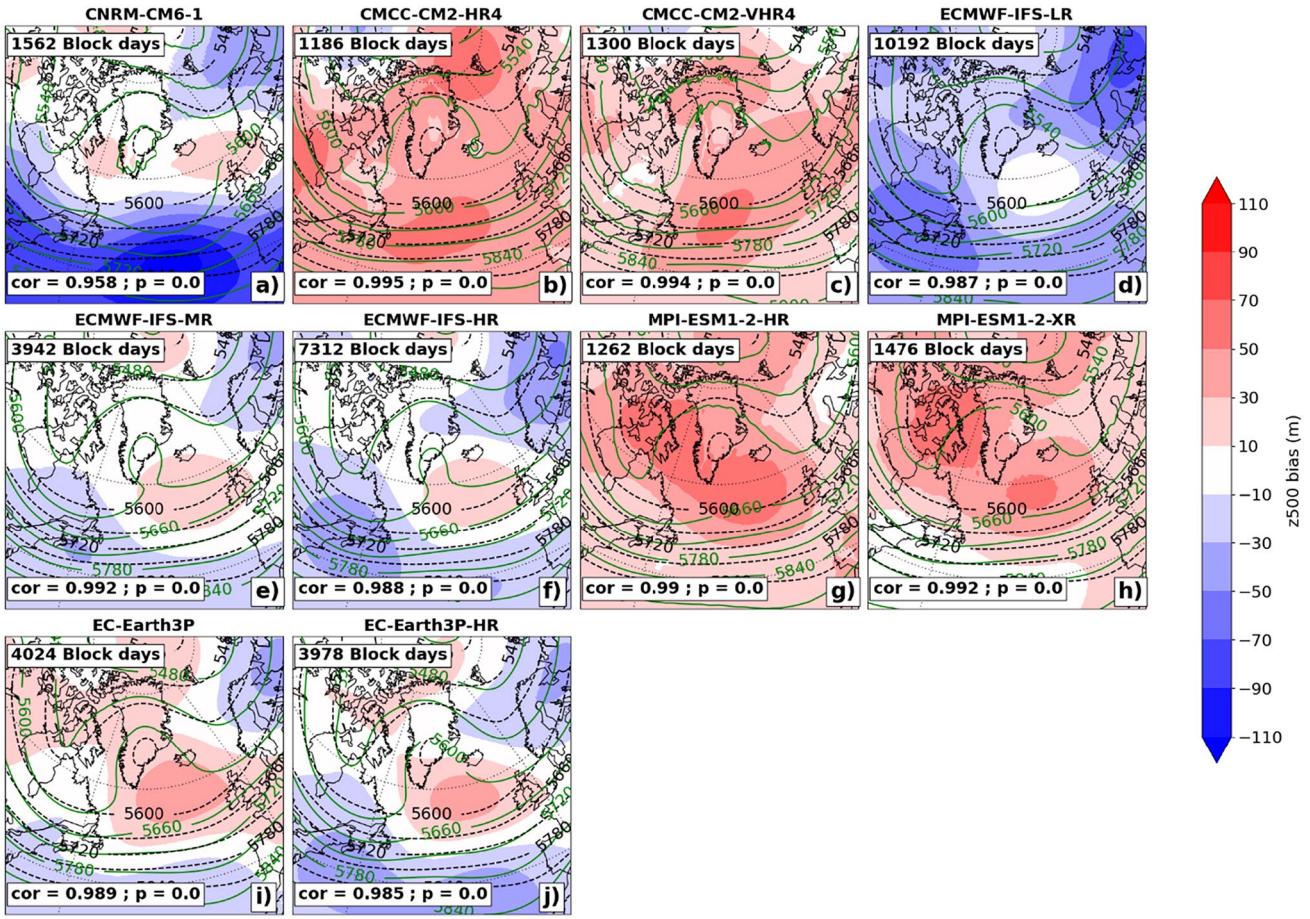

Fig. 3 Climatological mean of z500 for all blocking days from ERA5 (1950–2014, dashed black contours), all HighResMIP models (1950–2014, solid green contours) and their bias (shaded colors) compared to ERA5. The names of each dataset (and the number of members if any) are given on top of each panel. The Pearson pattern correlation coefficient between models and ERA5 over SOM domain and its p-value are shown at the bottom of each panel. Different realisations of each model are pooled together

stand-alone cut-off low acting over the North Atlantic rather than a real blocking high (Wazneh et al. 2021). If all three conditions are valid at a grid point and expand over at least 15 consecutive degrees of longitude centred at that grid point, we define it as a Large-Scale Block (LSB, as in Davini et al. 2012). Finally, a blocking event is determined if this LSB persists for at least 4 consecutive days at any grid points within a box of 5° latitude and 10° longitude centred on that grid point. Note that we only search for LSB over Greenland area (65–25°W and 60–75°N). Both GB2 and D12 indices are calculated for the summer (JJA).

2.3 Self Organising Map (SOM) for clustering blocking patterns.

Self Organising Map (SOM) is an unsupervised learning method for dimensionality reduction and extraction of different spatial patterns within data (Kohonen 1990, 2013) and has multiple applications in climate studies (Lennard and Hegerl 2015; Ohba et al. 2016; Odoulami et al. 2023; Gibson et al. 2017). Some climate studies found advantages of SOM in clustering patterns compared to a conventional K-Means clustering method (Lin and Chen 2006) and a standard principal component analysis (PCA) that fails to determine well-known patterns and can even mix different patterns into one component (Reusch et al. 2005). Similar to other learning algorithms, SOM requires a few parameters that must be provided beforehand by users, including the number of nodes (i.e., clusters or patterns) describing the structure of the SOM in a 2-D array, a given learning rate at which a specific SOM node is adjusted during the training, and a radius parameter for determining neighboring nodes of that SOM node and to scale down the learning rate used to adjust the neighboring nodes so that a further neighboring node receives a smaller learning rate. In principle, the SOM training process comprises a few steps. First, a 2-D SOM structure is selected and initialized using the first two principal components of all sample data. Second, a sample is randomly selected from the input database and the

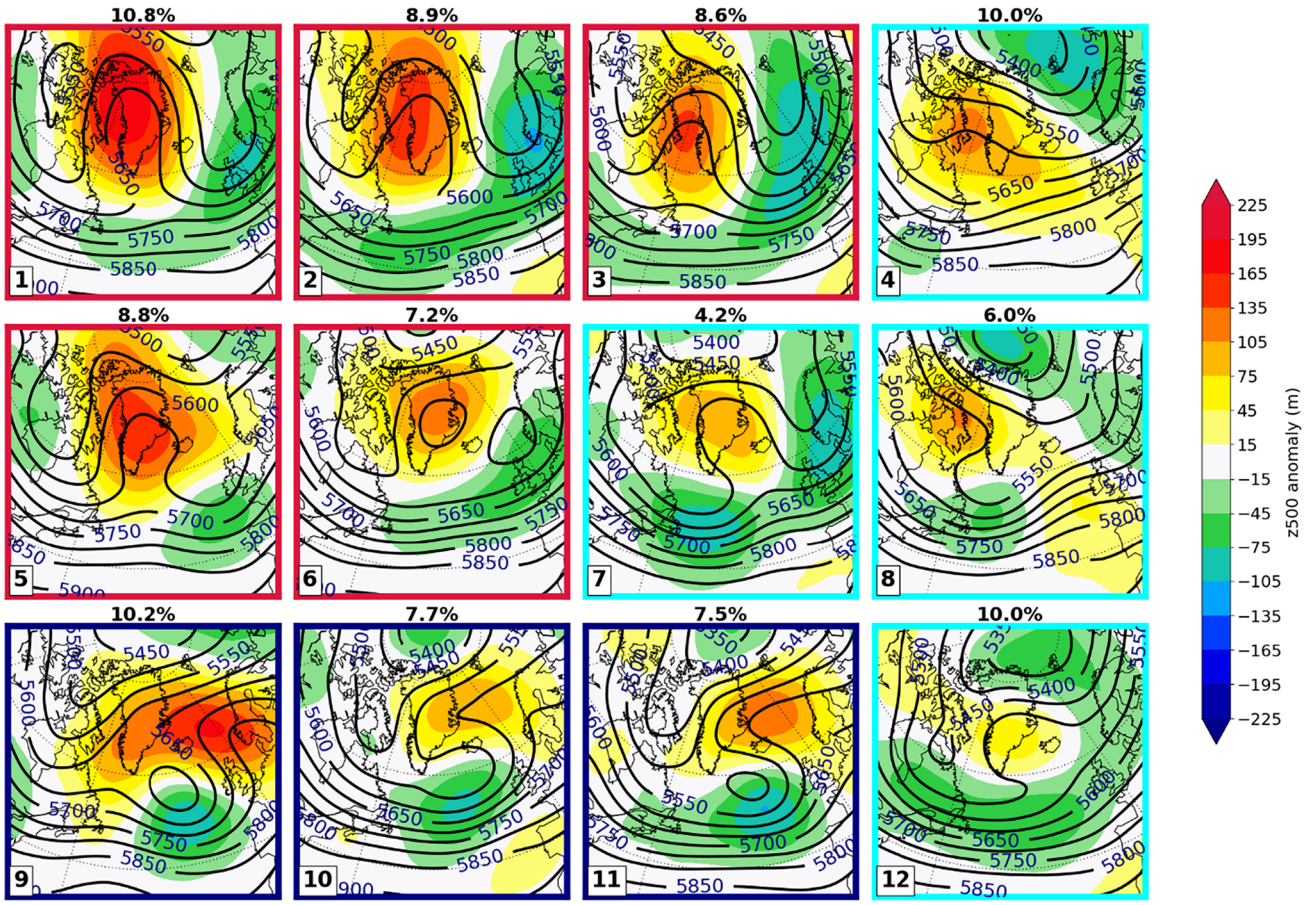

Fig. 4 Composite map of blocking patterns derived from SOM method applied to geopotential height at 500 hPa (z500) of 1424 JJA blocking days from ERA5 dataset for of 1950–2014. Contours show mean of z500, and shaded colors show its anomaly with respect to 1951–2000. The numbers in percentage on top of each panel denote the frequency of occurrence of each pattern. Similar plots for each model in HighResMIP are given in Supplementary document. The color of each panel frame, e.g., navy, cyan and red denotes the blocking pattern for cyclonic wave breaking structure (CWB), summer ridge (Ridge) and Omega blocking (Omega)

best matching unit (BMU) of that sample is determined by comparing the Euclidean distances between that input sample and those nodes in the SOM structure. Third, the BMU and its neighbors are adjusted to better resemble the input sample at different given rates governed by the learning rate and radius parameters. The second and third steps are repeated 100,000 times to get the final results.

In this study, we select a structure of three rows by four columns to perform the SOM analysis, similar to that carried out in Preece et al. (2022). For other SOM parameters, we choose a learning rate of 0.01, a radius of 2 and a 100,000 iteration of training steps. We apply the SOM to an extended domain of Greenland and North Atlantic covering 80°W–20°E and 40–85°N. This is applied to absolute z500 for all summer blocking days (as obtained by pooling all blocking days defined by criteria of either GB2 or D12 indices in Sect. 2.2) from the ERA5 database for the period of 1950–2014 to extract a set of master nodes that represent different atmospheric blocking patterns over Greenland. We then map each blocking day to one best matching master node (or blocking pattern) out of 12 nodes. Finally, we compute the average of all samples for each node to obtain the final climatological mean patterns for ERA5. For each model simulation, in order to facilitate comparison with ERA5, we also map z500 of each blocking day to those SOM master nodes and then take the node average (similarly to the ERA5 samples), rather than applying the SOM technique to every single model.

3 Results and discussion

3.1 Temporal evolution of Greenland blockings

Greenland blocking index (GBI and GB2) for summer is observed to strongly increase over the last 2–3 decades between the 1990s and 2010s; however, this increase is not reproduced in recent model climate simulations of CMIP5

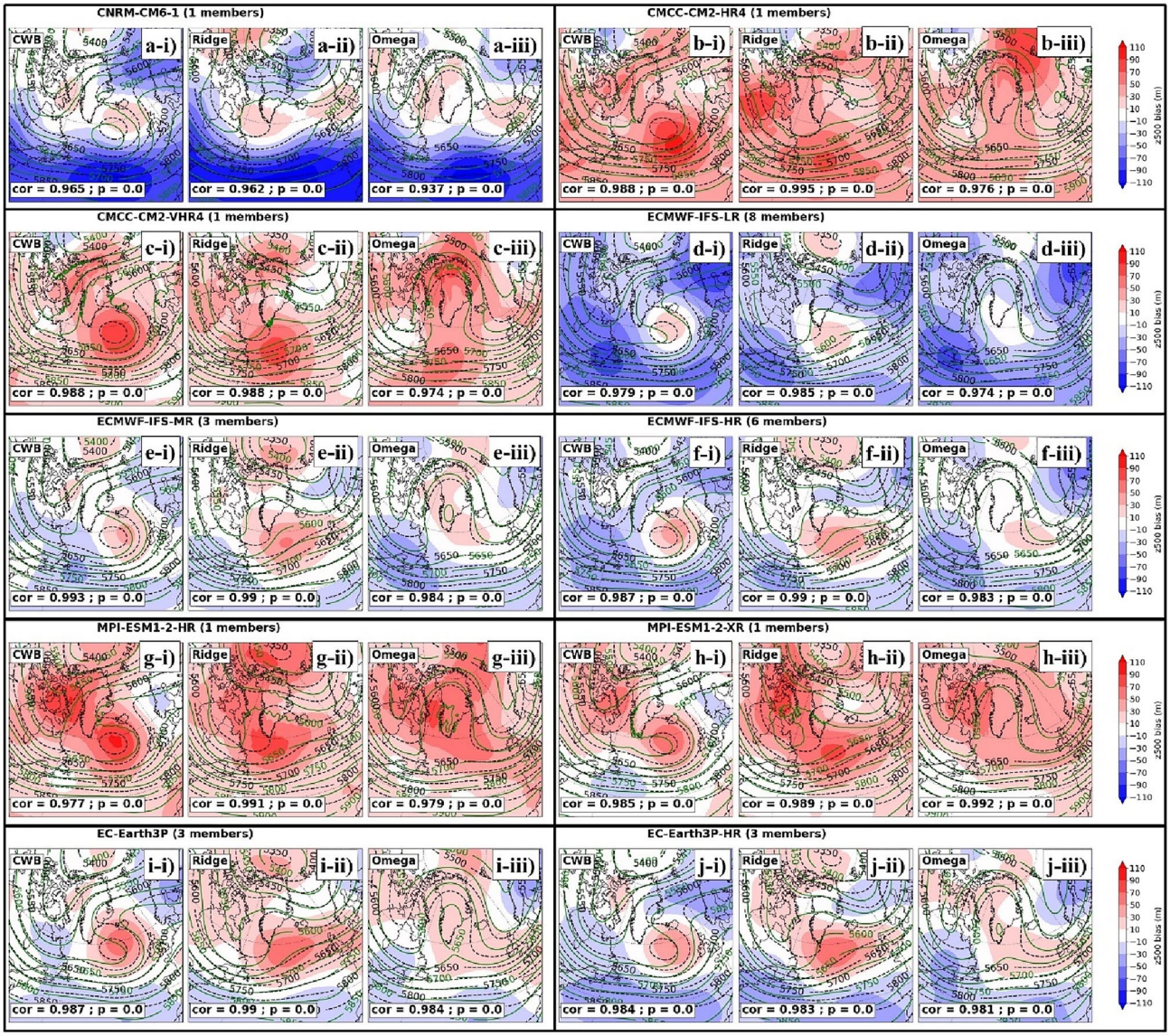

Fig. 5 Climatological mean of z500 for blocking patterns derived by grouping all SOM nodes into three main patterns, namely CWB (sub-panel i), Ridge (sub-panel ii) and Omega (sub-panel iii) from ERA5 (dashed black contours) and HighResMIP ensemble (solid green contours) for the period of 1950–2014. The shaded colour show mean biases of model compared to ERA5. The Pearson pattern correlation coefficient between models and ERA5 over SOM domain and its p-value are shown at the bottom of each panel

and CMIP6 (Delhasse et al. 2021; Hanna et al. 2018a; Maddison et al. 2024). Here, we quickly re-visit the temporal evolution of monthly GB2 over the summer from the ERA5 data up to and including summer 2023 and the HighResMIP model simulations for the historical period. Figure 1 shows time series of monthly mean GB2 for summer from all datasets that are smoothed by a 20-year window moving average. We find here that GB2 from ERA5 tends to increase sharply in 2 decades starting from the 1990s with its peak exceeding the previous highest value that was reached in the 1950s. However, the GB2 increase during that period seems to slow down after 2005 and it starts to decrease quickly over the recent few years (as shown by 11-years smoothing GB2 time series, Figure not shown here). However, HighResMIP simulations do not show a clear increase as observed, more rather showing weaker decadal variability throughout the whole period. There is one model, MPI-ESM1-2-XR, that shows a decadal increase in GB2 of similar magnitude to ERA5 but occurring about 10 years earlier. On the other hand, a member of ECMWF-IFS-HR model shows a sharp decrease in GB2 in the recent decades that also produces its minimum around the year 2000. These differences suggest

a high internal variability in the HighResMIP ensemble. On average, there is no trend and only weak decadal variability of GB2 values from the HighResMIP ensemble mean, implying a small forced component. We also note that there are no clear differences between different resolution versions of each model. A further discussion of trend and variability of GB indices using larger CMIP6 ensembles and other MIPs is presented in a complementary study (Maddison et al. 2024).

3.2 Distribution of Greenland blocking index (GB2)

In this section, we evaluate the distribution of daily GB2 values for all blocking days from all model simulations in comparison to ERA5 for the period 1950–2014. First, we select all blocking days satisfying the criteria of either GB2 or D12 indices (Sect. 2.2) for each database. For models with more than one member, we pool all GB2 values of all blocking days of all members together. We then plot each model GB2 distribution against the ERA5 distribution using the quantile–quantile (Q-Q) plot, a method to compare the quantiles of empirical distributions of two variables (Coles et al. 2001), as shown in Fig. 2. This method is particularly useful when visualizing and evaluating both tails (extremes) of the distribution. Furthermore, we embed a blue boxplot in the top left of each panel in Fig. 2 that shows the difference of quantiles of GB2 distribution between each model and ERA5. In other words, the boxplot shows the difference in GB2 value for each point in the q-q plot between model (ordinate) and ERA5 (abscissa). In an idealized case that model is near perfect, all points in the q-q plot would stay closely and along the diagonal line of each panel, while all boxplots would be centred around zero value. For Greenland blocking events defined using the GB2 index criteria only, all GB2 values from the distribution should be greater than 1 sigma (Appendix Fig. 9). By pooling all blocking days defined by either GB2 or those defined by D12 index, many blocking days with GB2 values smaller than 1 sigma are considered, and this is shown in Fig. 2. We also note that many blocking days with extremely high GB2 values, e.g.,

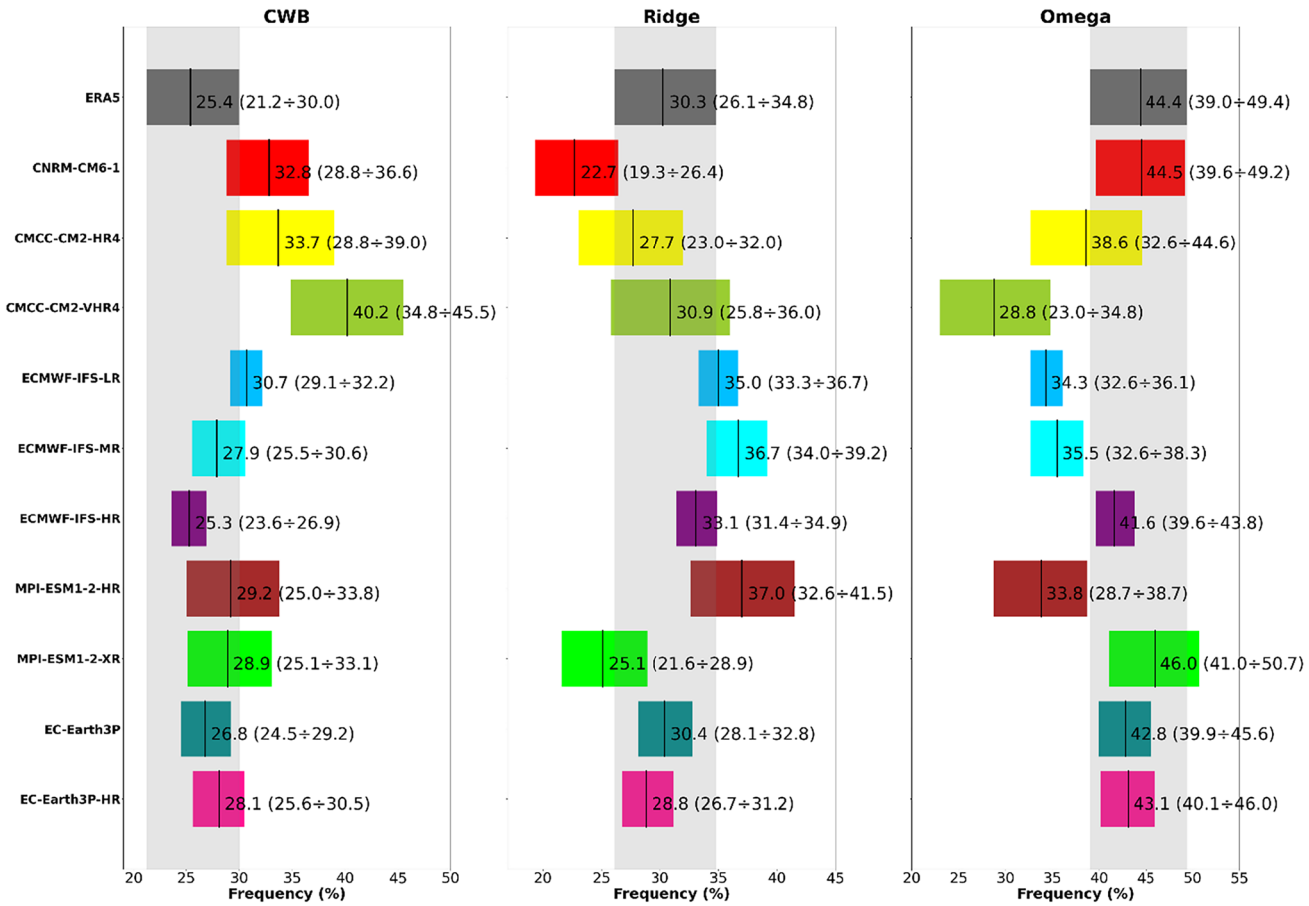

Fig. 6 Frequency of each blocking pattern from all datasets for the period of 1950–2014. The vertical black line in each box shows the mean frequency, while the box shows the 95% confidence interval computed using the bootstrapping method. The vertical transparent grey bar in each panel marks the 95% confidence of ERA5 dataset to facilitate the comparison of all models

between 3 and 4 sigma, are missed if we use only the D12 index (Appendix Fig. 10). All models reproduce GB2 values well for a range from + 1 to 2 sigma, except the CNRM-CM6-1 model which completely underestimates the distribution of GB2 including both tails beyond 0.5 sigma (Fig. 2a). Two versions of CMCC-CM2 underestimate GB2 values by up to – 0.4 sigma for GB2 above + 2 sigma, and overestimate by up to 0.5 sigma for those GB2 value below + 1 sigma (Fig. 2b and c). The two versions of MPI-ESM1-2 show different behaviours. The lower resolution version slightly overestimates GB2 for the upper tail (above + 3 sigma) and underestimates GB2 in the lower tail (below + 1 sigma, Fig. 2g), while the higher-resolution version simulates both these tails well but underestimates GB2 for the rest of the distribution (Fig. 2h). The rest of the models, namely the three versions of the ECMWF model and the EC-Earth model, closely simulate the distribution of GB2, with their bias close to 0 (Fig. 2d, e, f, i and j). The three ECMWF models and EC-Earth share the same atmospheric component Integrated Forecasting System (IFS) with the ERA5, which could explain the relatively good performance. However, for the MPI-ESM1-2, the lower atmospheric resolution version (HR) outperforms its higher resolution version (XR, Fig. 2g and h, respectively). We note here that the GB2 is a normalized index that has largely nullified the impact of thermodynamic changes (by subtracting the spatial mean state of z500 over mid-latitude regions), and standardized by its own standard deviation of each model, thus largely removing systematic bias in mean state of the flow in the model that would otherwise alter blocking climatology (Scaife et al. 2010).

3.3 Spatial pattern of Greenland blockings

In this section, we evaluate the mean bias of z500 from HighResMIP in reproducing the climatological mean of all summer blocking days obtained from the combination of all events defined by either GB2 or D12 indices (Fig. 3,

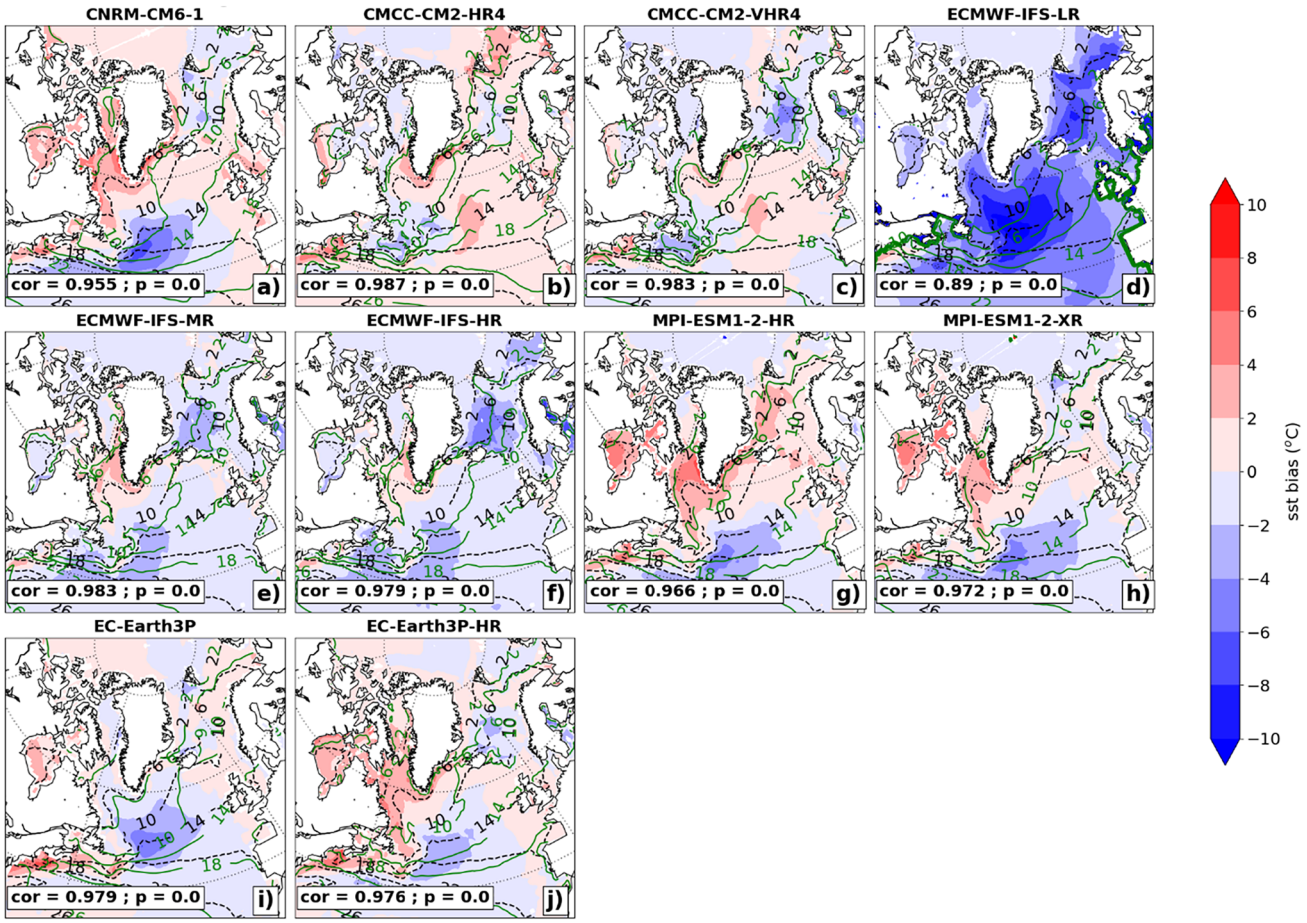

Fig. 7 Climatological mean of sea surface temperature (°C) for the summer (JJA) from ERA5 (black dashed contour) and all climate models (green solid contour) used in this study and their bias (shaded colour) compared to ERA5, for the period 1950–2014. The Pearson pattern correlation coefficient between models and ERA5 over SOM domain and its p-value are shown at the bottom of each panel. Different realisations of each model are pooled together

absolute values of climatological mean and their anomalies are shown in Fig. 11), in comparison with ERA5. For each model with more than one member, we pool all the members and take the mean of all realisations. In general, all models can reproduce well the position and spatial pattern of summer blocking over Greenland. Specifically, the pattern correlation coefficients, i.e., spatial correlation of climatological mean of z500 field between models and ERA5 over the SOM domain (80°W–20°E and 40–85°N.) revolve around 0.99, except for CNRM-CM6-1 with correlation coefficient of 0.958, and all are statistically significant. The centre of high-pressure system from ERA5 is located over southern Greenland (between 65 and 70°N). Half the models, including the medium- and high-resolution versions of ECMWF-IFS, CNRM-CM6-1 and 2 versions of EC-Earth3P, reproduce well this feature with bias of z500 ranging from – 10gpm to 30 gpm but they underestimate z500 over Scandinavia and central north Atlantic (from 50°N and further south) regions from -10gpm to -30gpm, except the CNRM-CM6-1 which has a negative bias reaching – 110 gpm. Meanwhile the other GCMs, including 2 versions of CMCC-CM2 and MPI-ESM1-2, generate the blocking with positive biases ranging from 30 to 50 gpm. These two models also overestimate z500 over the whole domain by a similar bias range. The ECMWF-IFS-LR is the only model underestimating z500 over the whole domain by – 10 to – 70gpm. All the models show a positive blocking bias over the sea to the southeast of Greenland extending to off the west coast of the UK. This feature remains the same when considering the bias in anomaly of z500 in the models (Appendix Fig. 12). However, for other areas, the bias in z500 anomaly is smaller in the model, even for those models with large negative bias such as CNRM-CM6-1 and ECMWF-IFS-LR. In addition, we check the bias field of z500 for all non-blocking days during the summer, which shows a very similar bias pattern to all blocking days, except for the positive bias pattern to the southeast of Greenland (Fig. 13). This suggests that the bias in the mean of absolute z500 is rather systematic. However,

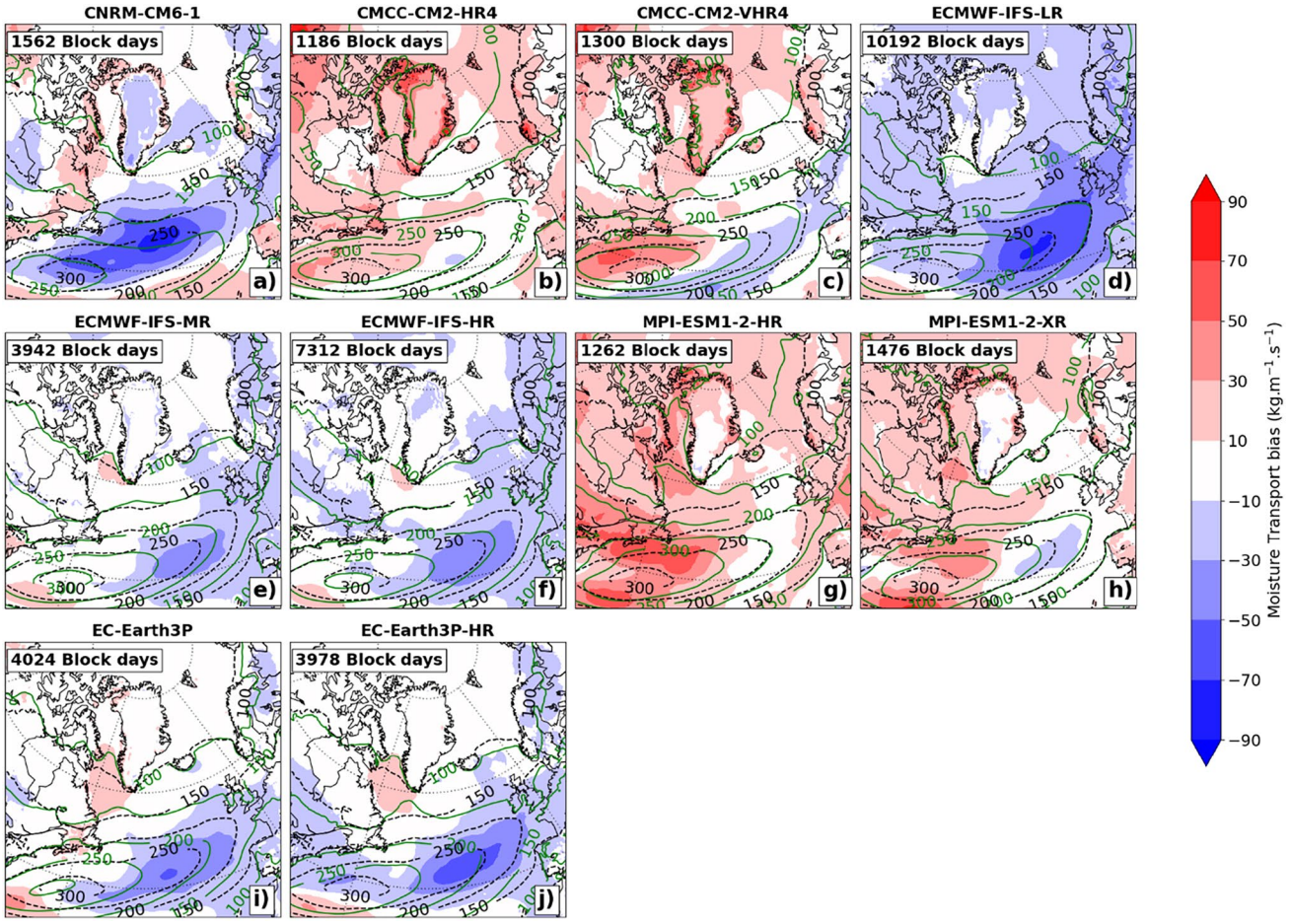

Fig. 8 Climatological mean of moisture transport ($kg.m^{-1}.s^{-1}$) for all Greenland blocking days from ERA5 (black dashed contours) and all climate models (green solid contours) used in this study and their biases (shaded colors), for the period 1950–2014. For those contours, online moisture transport values greater than 100 $kg.m^{-1}.s^{-1}$ are plotted. Different realisations of each model are pooled together

we do not find any clear advantages of higher resolution in reproducing blocking intensity over Greenland from this HighResMIP ensemble.

Both the position and large-scale patterns of blocking over Greenland have a dominant impact on moisture transport, cloud cover, surface ice melting and surface energy fluxes leading to changes in the surface energy balance and mass balance of the Greenland Ice Sheet (Ward et al. 2020; Preece et al. 2022; Hermann et al. 2020). Here, we investigate different spatial patterns of all the GB episodes that are detected using GB2 and D12 indices. Figure 4 shows composite maps of the twelve different nodes obtained using SOM analysis for ERA5. The contour lines show absolute z500 and the shaded colors show its anomaly with respect to 1951–2000 climatological mean. The SOM technique reproduces the three main blocking patterns mentioned in Sect. 1. Nodes 9, 10 and 11 show a cyclonic wave breaking structure (hereafter denoted as CWB) when a high-pressure system moves westward from the Scandinavian region and retrogrades to Greenland over the poleward flank of a cut-off low at lower latitudes. We highlight those panels by navy boxes in Fig. 4. Nodes 4, 7, 8 and 12 (cyan boxes) represent the summer ridge pattern (Ridge) that develops from the North Atlantic and extends over the southern part of Greenland. The rest of the nodes (red boxes) describe the omega blocking pattern (Omega), which has closed contour height lines over Greenland and a higher intensity in comparison with the Ridge pattern. These spatial patterns are consistent with those found in Preece et al. (2022), though the SOM parameters, domain and period of data in our study might be different (their exact choice of parameters are not specified). This supports the robustness and reliability of our method and classification results. In addition to this ERA5 analysis, we also apply similar procedures which map all blocking episodes to their best matching one among 12 master nodes derived from the SOM analysis of ERA5 to obtain twelve node-averages for each HighResMIP simulation (not shown here).

In order to simplify the evaluation of those models, we reduce the dimensionality of the SOM by taking the mean of all nodes showing the same three patterns: namely CWB, Ridge and Omega. The results of this analysis are shown in Fig. 5. In general, all models can reproduce the spatial distribution of blocking for all patterns, as well as the position of the cut-off low associated with the CWB pattern and two low areas for the Omega pattern. This is quantified by high pattern correlations, i.e., from 0.95 to 0.99, which are all statistically significant. Models can also capture the fact observed from ERA5 that z500 anomalies over Greenland are largest for the Omega pattern (sub-panel iii in Fig. 5a–i), and smallest for the Ridge pattern (sub-panel ii in Fig. 5a–i). For the absolute magnitude of z500, models tend to produce biases with similar signs (e.g., positive, or negative) for all three patterns. For example, the two versions of CMCC-CM2 and MPI-ESM1-2 overestimate z500 in the blocking high area over Greenland for all three patterns (Fig. 5b, c, g and h), while the ECMWF-IFS-LR underestimates it over the whole domain for those patterns (Fig. 5d). This means that a systematic bias exists which, to first order, is independent of blocking patterns. We find that the magnitude of the z500 biases for all patterns, especially over blocking high areas and their associated low systems, are smaller in the higher-resolution version of each model, but this slight difference is negligible, except for the ECMWF-IFS-LR compared to its higher resolution versions (Fig. 5d). This is consistent with what was previously found regarding the uncertain improvement of higher-resolution models for summer blocking in midlatitude regions (Davini and D'andrea 2020). We also note that in this HighResMIP ensemble, only two models – the ECMWF-IFS (Fig. 5d–f) and EC-Earth3P (Fig. 5i–j) – have both higher and lower-resolution of ocean components among their members (0.25° and 1° horizontal resolution as shown in Table 1). The improvement in z500 simulation results is obvious for the former model, especially since ECMWF-IFS-LR (Fig. 5d) and ECMWF-IFS-MR (Fig. 5e) share the same-resolution atmosphere component. This suggests a role of ocean model in coupling with the atmosphere. Meanwhile, the EC-Earth3P-HR (Fig. 5j) uses higher resolution for both its atmosphere and ocean components but shows no obvious improvement in its ability to simulate Greenland Blocking patterns.

3.4 Frequency analyses for blocking patterns

In this subsection, we evaluate the ability of HighResMIP models to reproduce the relative frequency of each of the previously specified Greenland blocking patterns. For each dataset, we count the number of summer blocking days in each pattern. In addition, we use a non-parametric bootstrapping method (Von Storch and Zwiers 2002) to estimate the 95% confidence interval of relative frequency of each blocking pattern for each dataset. First, we randomly pick blocking events, of which each event consists of several consecutive blocking days determined by either GB2 or D12 criteria, with replacement for a bootstrap sample until the size of that bootstrap sample is equivalent to the original sample size. Then, we classify all blocking days from that bootstrap sample into the main three blocking patterns using the procedure discussed in previous sections to obtain the frequency for each pattern. We repeat this sampling procedure 1000 times and then compute the 95% confidence interval. Figure 6 shows the frequency of occurrence of each blocking pattern for all datasets. The ERA5 reanalysis shows that the omega pattern occurs 50% more frequently

than ridge and 75% more frequently than the CWB. Specifically, CWB occurs on 25.4% (21.2–30%) of the total number of blocking days, while the ridge and omega patterns occur on 30.3% (26.1–34.8%) and 44.4% (39–49.4%) of the days, respectively. Most models can reproduce these frequencies of patterns to some extent, e.g., their 95% confidence interval overlapping with the interval from ERA5, except the CMCC-CM2-VHR4, MPI-ESM1-2-HR, ECMWF-IFS-MR and ECMWF-IFS-LR which all underestimate the frequency of omega pattern leading to a higher proportion of ridge and CWB patterns in those models relative to the observed frequencies. Specifically, the CMCC-CM2-VHR4 overestimates CWB frequency by 15% and underestimates omega pattern by 16%. The MPI-ESM1-2-HR, ECMWF-IFS-MR and ECMWF-IFS-LR underestimate the frequency of the omega pattern by roughly 10–12%. Again, we find here that the model errors in the relative frequency of the different blocking patterns are not subject to model resolution. The higher-resolution models can still lead to larger biases in frequency.

3.5 Potential sources of biases in the simulations of Greenland blocking.

Here we investigate the bias of summer mean SST simulated by HighResMIP models compared to ERA5 (Fig. 7). There is a large southeast-northwest SST gradient over the North Atlantic towards the Labrador Sea, Baffin Bay, and Greenland Sea from the ERA5 (black dashed contours in all panel of Fig. 7). This SST gradient is especially sharp over the Gulf Stream. All models generally reproduce these features and the SST distribution over this region; however, the mean biases are large (with an absolute bias up to 10 °C) for some models. For CMCC-CM2 and MPI-ESM1-2, the two versions of each model share the same spatial resolution of their ocean component, and the SST bias between the two versions is consistent (Fig. 7b, c, g and h). CMCC-CM2 shows a cold bias over Baffin Bay, the Labrador Sea, along the east coast of US and Canada, and over the Greenland Sea (Fig. 7b). The bias is larger (– 4 to – 6 °C) in CMCC-CM2-VHR4: the higher atmospheric resolution version (Fig. 7c). Meanwhile, this model overestimates SST (0–4 °C) around the southern coast of Greenland and further south in the North Atlantic. MPI-ESMI-2 shows an opposite SST bias pattern. While a warm bias (2–4 °C) occurs over regions to the west of Greenland, the model underestimates SST by up to 6 °C over the central North Atlantic (Fig. 7g and h). The MPI-ESM1-2-HR model also overestimates Greenland Sea SST; meanwhile MPI-ESM1-2-XR (with a higher-resolution atmospheric component) slightly underestimates SST over this region. These model biases suggest that the coupling mechanism and sea-air interaction within the models play an important role in modulating SST over this area. For ECMWF-IFS and EC-Earth3P, which have different resolutions of their ocean components, the SST biases are different for different versions. The coarser resolution of EC-Earth3P shows slight cold bias (0 to – 2 °C) over Baffin Bay and the Labrador and Greenland Seas but largely underestimates SST (with model biases reaching between – 6 and – 8 °C) over the central North Atlantic (Fig. 7i). In contrast, the EC-Earth3P-HR overestimates SST from 0 to 4 °C over regions to the west of Greenland (Fig. 7j). The ECMWF-IFS-LR largely underestimates SST all over the plotted domain, with model biases of up to between – 8 and – 10 °C (Fig. 7d). The other versions of ECMWF-IFS (which share the same resolution ocean component) also underestimate SST (mostly between 0 and – 4 °C) over most areas in this domain, except along the southern coast of Greenland (Fig. 7e and f). The ECMWF-IFS-HR produces a larger cold bias over the Greenland Sea compared to the ECMWF-IFS-MR, which shares the same resolution ocean component but has a coarser-resolution atmosphere component. Finally, the CNRM-CM6-1 (Fig. 7a) shows a very similar bias pattern and magnitude to MPI-ESM1-2-XR (Fig. 7h). However, the biases in the mean state of z500 during Greenland blocking days are completely opposite between these two models, especially over the north Atlantic. This suggests that the impact of SST on blocking through coupling air-sea interaction in HighResMIP is model-dependent and needs to be further investigated (Davini and D'andrea 2016).

We further analyse the bias of daily mean moisture transport over all summer Greenland blocking days from ERA5 and HighResMIP ensemble (Figs. 8 and 14). The moisture transport is a vertically integrated product of horizontal wind vectors and specific humidity from 1000 to 500 hPa following the method used in Barrett et al. (2020) and Mattingly et al. (2016). The ERA5 spatial pattern shows that moisture is transported from the Hudson Bay upstream towards northern Greenland and turns into northwesterly flow on the leeside of Greenland (Fig. 14a). This is consistent with the spatial pattern of geopotential height shown in Fig. 3. The southwesterly moisture flow is maximized around 80°W and 40°N over the northwest Atlantic and bends southwards around the North Atlantic subtropical high. All HighResMIP models tend to reproduce well these spatial features of moisture flow. However, the two models CMCC-CM2 and MPI-ESM1-2 (both high and coarse resolution versions) largely overestimate the magnitude of moisture transported into Greenland as well as the northwest Atlantic where moisture content is maximum (Fig. 8b, c, g and h). Meanwhile, the remaining HighResMIP models either reproduce well or slightly underestimate moisture transport around Greenland and underestimate the moisture to a higher extent over the central and eastern North Atlantic. Those models, except for ECMWF-IFS-LR (Fig. 8d), also slightly overestimate this quantity to the southwest of Greenland. These bias patterns

are consistent with the SST bias pattern, especially on the upstream side of Greenland extending to the Northwest Atlantic. The overestimation of SST over those areas might add extra moisture content into the boundary layer. Furthermore, these bias patterns of moisture transport are coherent with the mean bias of z500 over all summer Greenland blocking days in Figs. 3 and 5.

3.6 Discussion

GB2 is a modified version of Greenland Blocking Index (GBI) that is purely an area-weighted average of z500 over Greenland. Although the impact of thermodynamic changes due to regional temperature increase or seasonality is eliminated from GB2, we still find here a consistent increase of this index for the summer in the last few decades, similar to recent GBI trends noted in previous studies (Hanna et al. 2016, 2018a, 2018b). Hanna et al. (2018a) suggested that regional changes in atmospheric temperature could not be the only driver of that increase in summer GB2. This increase might relate to the positive phase of Atlantic Meridional Oscillation (AMO+) in combination with the positive North Atlantic tri-pole pattern that together can enhance warmer sea surface conditions over high latitudes (Wang and Luo 2022). The GB2 increase might also relate to a more highly amplified Northern Hemisphere jet stream that has previously been noted. Such an amplified jet stream could relate to anthropogenic climate change (Overland et al. 2012). However, GB2 only reflects one aspect of GB episodes, while using other indices, e.g., D12 index or the gradient of potential temperature on the dynamical tropopause (Pelly and Hoskins 2003), can lead to different results (Pinheiro et al. 2019; Wachowicz et al. 2021). We also find that the number of Greenland blocking days in the summer defined by D12 index tends to increase significantly by 1.34 days/decade over the whole period of ERA5 (1940–2023), while the number of blocking days defined by GB2 increases by a lower rate (0.57 days/decade) and is not statistically significant (Appendix Fig. 13). In line with that, Barrett et al. (2020) show that summer extreme daily GBI happens more frequently in recent decades. Preece et al. (2022) also reveal stronger Greenland blocking patterns like Omega and CWB tends to happen more frequently in recent decades, especially since the year of 2000. This might also explain strong increasing trend of GB2 after that year. However, it is disclosed in Maddison et al. (2024) that this sharp increasing trend in GB2 is not sustained and rather a demonstration of decadal variability.

Sea surface temperature (SST) has a large impact on the atmosphere through air-sea coupling (Wills et al. 2016; Ossó et al. 2019, 2018). Over the Atlantic, SST biases can influence the mean bias of the atmosphere and therefore affect model representation of blocking (Scaife et al. 2011). In addition, a sharp SST gradient can modulate the lower tropospheric poleward eddy heat transport and enhance upper-level eddy kinetic energy, bracing the stationary jet and intensifying atmospheric blocking (O'reilly et al. 2016; Famooss Paolini et al. 2022). Novak et al. (2015) suggest that the cyclical spatiotemporal evolving of these eddy fluxes, underpinned by the baroclinic environment, are associated with a steering either northward or southward of the jet and Rossby wave breaking over the North Atlantic. Mathews and Czaja (2024) find that oceanic heat content transported from the Straits of Florida extending along the Gulf Stream and its interaction with atmospheric boundary layer is associated with blocking over the north Atlantic. Maddison et al. (2024) show SST could play a role in Greenland blocking indices long term trend and variability. Our analysis of SST for HighResMIP models suggest there could be reflection of bias in SST into the bias of z500 field, hence the magnitude of Greenland blocking. However, this is subject to the coupling mechanism, and is therefore model-dependent. This finding is in line with the results of Davini and D'andrea (2020).

Moist dynamics play an important a role as dry dynamics in the formation and maintenance of atmospheric blocking (Maddison et al. 2020, 2019; Yamamoto et al. 2021). The latent heat released from vertical motion and cloud formation transports low potential vorticity (PV) air to the upper troposphere, producing negative PV anomalies that can trigger and intensify blocking (Steinfeld et al. 2020; Steinfeld and Pfahl 2019). Barrett et al. (2020) show that extreme GBI events are preceded by extreme moisture transported toward Greenland up to 2.5 days in advance in the summer. Hauser et al. (2024) find that moist processes associated with the warm conveyor belt plays an important role in amplification and maintenance of negative PV anomaly during blocking and supports the westward retrograding of this anomaly toward Greenland from Europe region. Our study uses moisture transport as a proxy of moist dynamic and latent heat fluxes released from cloud processes. The spatial pattern of moisture transport bias over the North Atlantic and Greenland areas are consistent with bias pattern of z500 during blocking days. This suggests an impact of model-simulated moist dynamics on the representation of blocking magnitude over Greenland.

4 Conclusions

Climate models have often struggled to adequately simulate some key elements of atmospheric blocking, especially its frequency and persistence. In this study, we take a closer look at atmospheric blocking over the Greenland region using the state-of-the-science ERA5 reanalysis spanning

from 1940 to summer 2023. We also employ the HighResMIP ensemble of high-resolution coupled models spanning 1950 to 2014 and evaluate the ability of those models to represent Greenland blocking. We use a number of different methods to understand different features in time, space, and distribution of those Greenland blocking events and to facilitate the evaluation of HighResMIP model simulations.

The time series of summer GB2 shows a sharp increase between the 1990s and 2010s, with its peak breaking the record of the middle of the twentieth century. However, the HighResMIP models fail to reproduce this temporal feature and show a high internal variability. We also show that most models can fairly reproduce the statistical distribution of daily GB2 values from all Greenland blocking events, especially those models sharing the dynamical core with the IFS in ERA5 and except the CNRM-CM6-1 which has a very coarse resolution atmosphere component compared to other models in HighResMIP.

Most HighResMIP models can reproduce the spatial pattern of Greenland blocking, for both the climatological mean of all events and for individual patterns such as the Omega type, summer ridge and Rossby wave breaking structure. The systematic biases of z500 magnitude in the model appear to be independent of blocking type. We find large SST biases over the North Atlantic and seas surrounding Greenland, and biases in moisture transport over the North Atlantic toward Greenland, especially over the western flank of blocking areas, which might together contribute to model biases in the representation of z500 magnitude during blocking episodes over Greenland. This also highlights the importance of coupling mechanism of ESM in blocking simulation. We also find here that the relative frequency of each blocking pattern is simulated well by most models, e.g., omega blocking is the dominant type over Greenland. This suggests potential use of these models in further impact studies of Greenland blocking on ice sheet melting and ice mass balance over Greenland, and extreme weather and climate over it and surrounding regions, which have different responses to different Greenland blocking patterns. However, we do not find that the higher-resolution models examined here have a clearly superior representation of summer blocking over Greenland. We also consider that a few forcing terms, e.g., aerosols and land-use cover, are simplified in HighResMIP (Haarsma et al. 2016), which may cause disparities in their historical climate simulations relative to ERA5. Therefore, the model-evaluation methods used in this study should be applied more widely to different MIPs in the CMIP6, e.g., DAMIP and PAMIP, to explore the impact of various forcings (in particular oceanic forcing) on model representation of the interannual variability of Greenland Blocking.

Appendix

Appendix A

See Figs. 9, 10, 11, 12, 13, 14, 15.

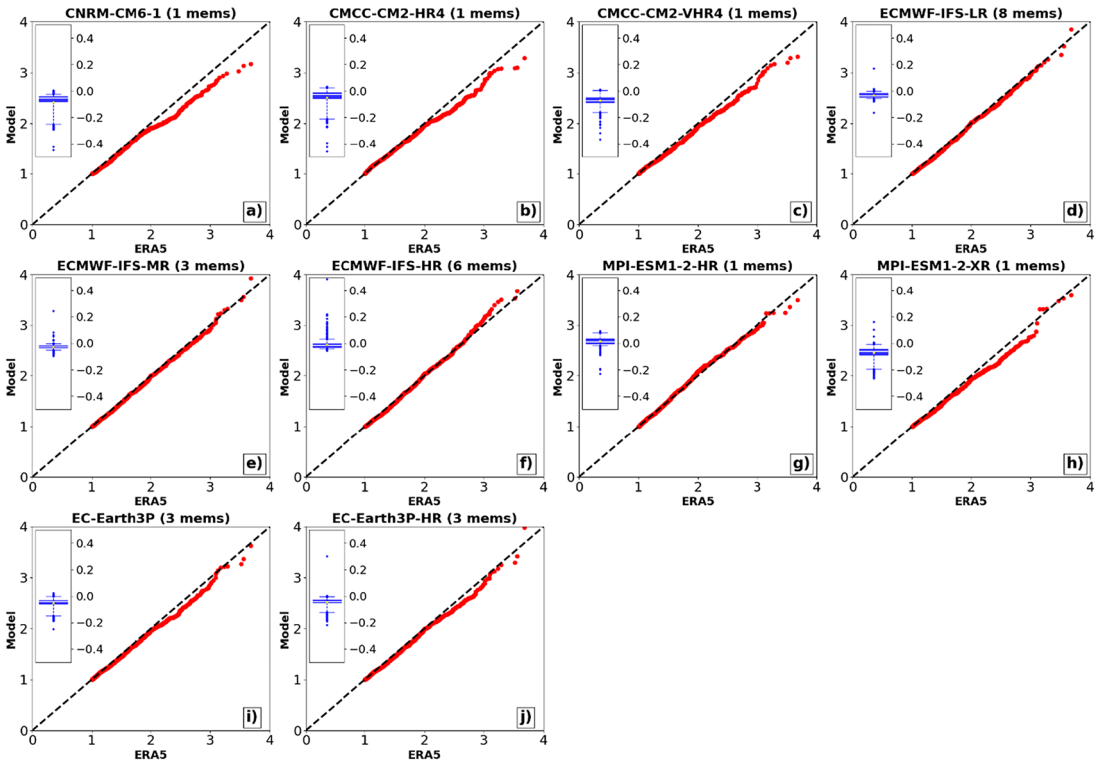

Fig. 9 Quantile–Quantile plot of GB2 values of all summer blocking days defined by using only GB2 index between ERA5 (1950–2014) and all HighResMIP models (1950–2014). All members from the same GCM are pooled together. The boxplot embedded within each panel shows difference of GB2 values between model and ERA5. The box shows interquartile range (25th to 75th percentiles), the whiskers show a range of 5th to 95th percentiles, and those outliers are extreme points outside the whisker range

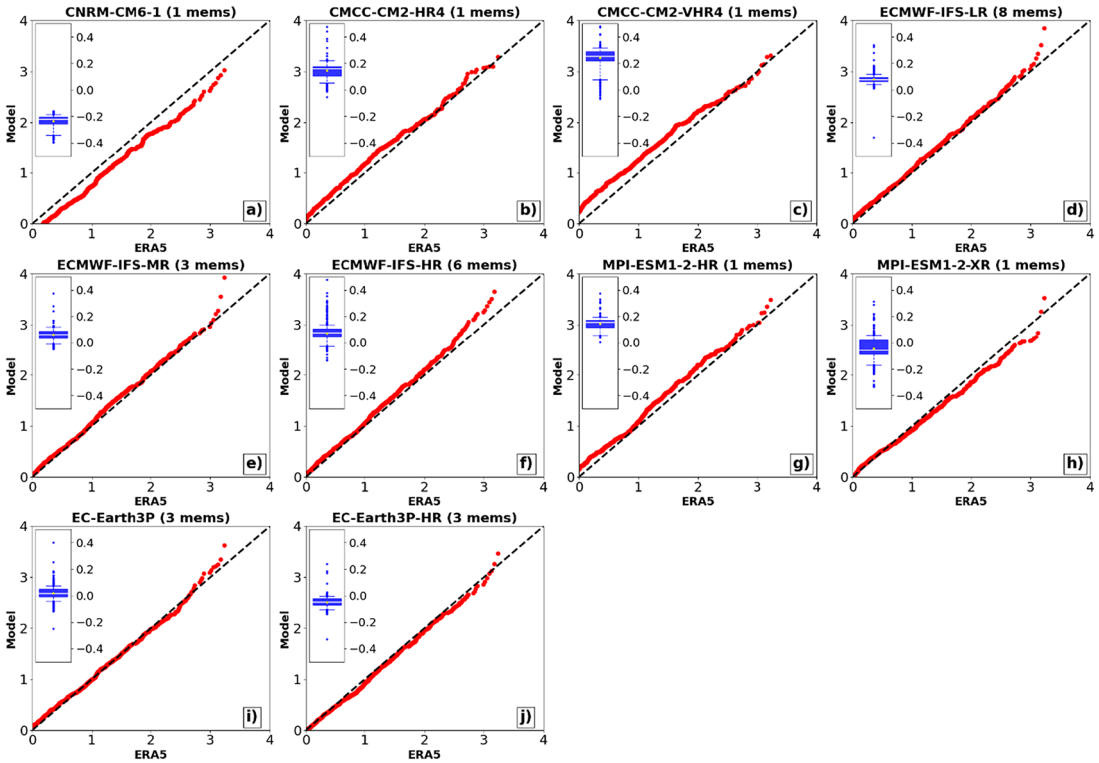

Fig. 10 Similar to Fig. 9 but using D12 only to define blocking events

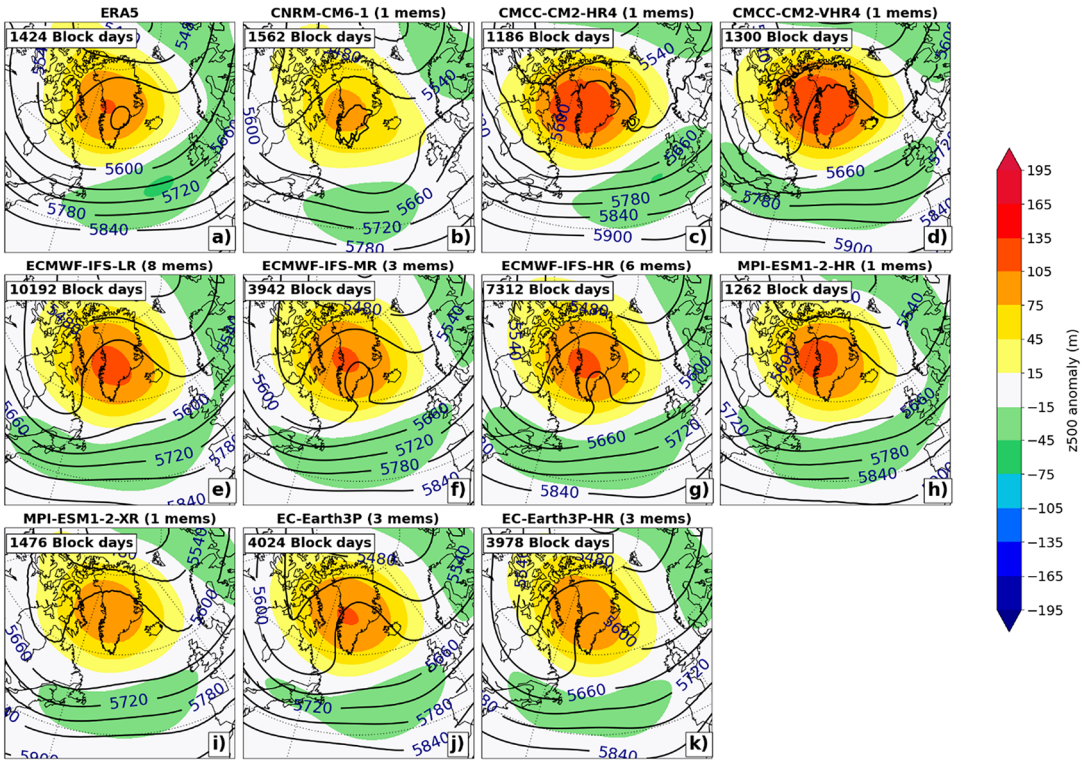

Fig. 11 Climatological mean of geopotential height at 500 hPa (z500) of summer blocking days from ERA5 (1950–2014) and HighResMIP models (1950–2014). Contours show mean of z500, and shaded colors show its anomaly with respect to 1951–2000

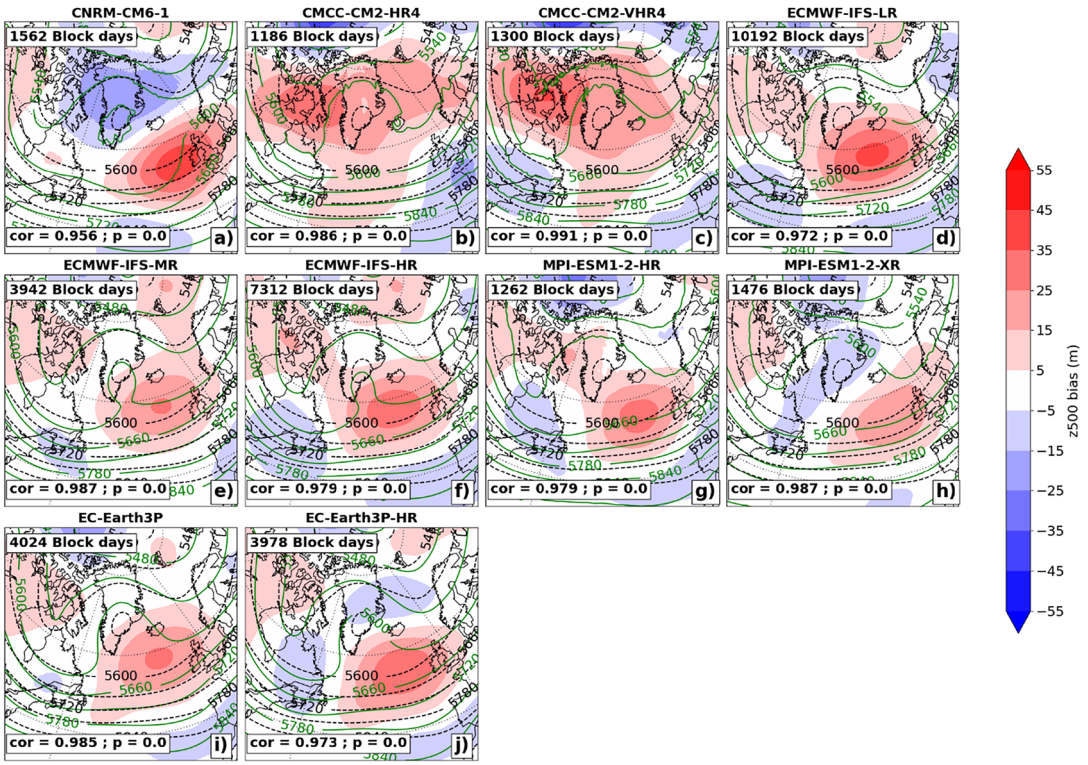

Fig. 12 Climatological mean of z500 for all blocking days from ERA5 (1950–2014, dashed black contours), all HighResMIP models (1950–2014, solid green contours) and the bias of z500 anomaly (shaded colors) compared to ERA5. The names of each dataset (and the number of members if any) are given on top of each panel. The Pearson pattern correlation between models and ERA5 over SOM domain and its p-value are showed at the bottom of each panel. Different realisations of each model are pooled together

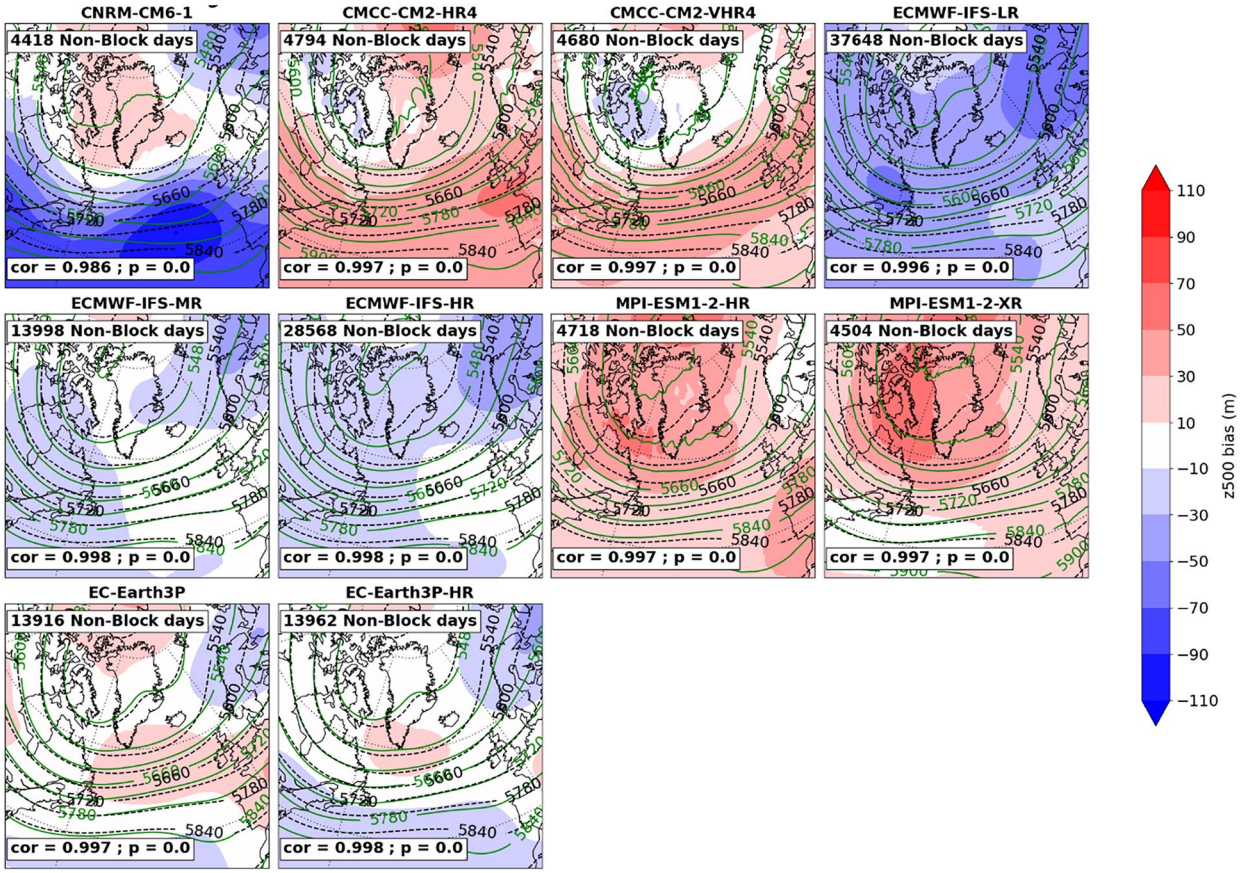

Fig. 13 Similar to Fig. 12, but for non-block days and bias of absolute z500

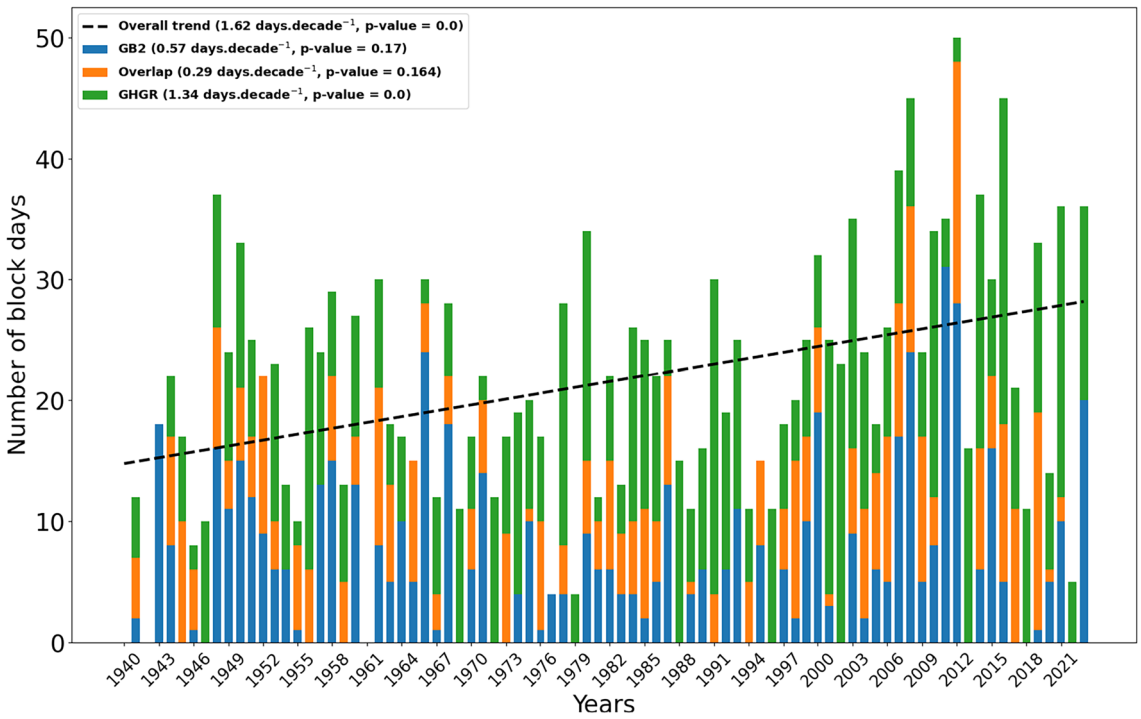

Fig. 14 Number of summer blocking days over Greenland defined by GB2 (blue plus orange) index, D12 index (green plus orange) and the overlap of the two indices (orange) from ERA5 dataset from 1940 to 2023

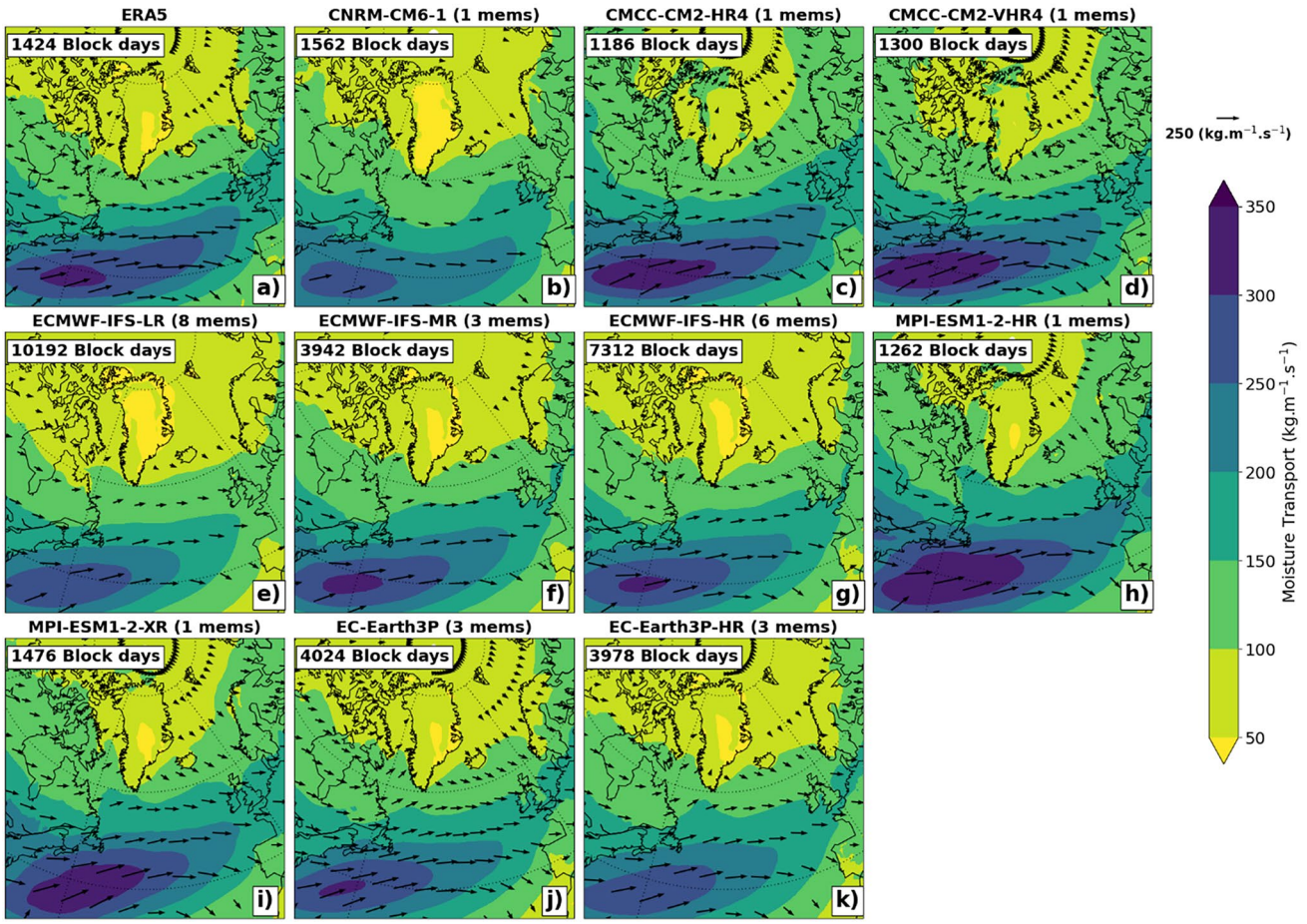

Fig. 15 Mean of moisture transport vector and magnitude (shaded colors, $kg.m^{-1}.s^{-1}$) for all summer blocking days defined by either D12 or GB2 indices from ERA5 and all HighResMIP models for 1950–2014

Acknowledgements This work was supported by NERC grant number NE/W005875/1. All analyses in this work were done using computing resources from the UK's data analysis facility for environmental science (JASMIN, https://jasmin.ac.uk/).

Author contributions Linh N. Luu and Edward Hanna conceived and designed the study with input from James Screen and Dilkushi de Alwis Pitts. Linh N. Luu collected all data with helps of Jacob Maddison, conducted all analyses and drafted the manuscript. All authors contributed to discussion of results, commenting, and editing the manuscript.

Funding This work was supported by NERC grant number NE/W005875/1.

Data availability The HighResMIP climate simulation data are extracted from the World Climate Research Programme (https://esgf-index1.ceda.ac.uk/search/cmip6-ceda/). The reanalysis data ERA5 is available on Copernicus Climate Data Store (https://cds.climate.copernicus.eu/cdsapp#!/home).

Declarations

Conflict of interest The authors declare that there is no conflict of interests.

References

Anstey JA, Davini P, Gray LJ, Woollings TJ, Butchart N, Cagnazzo C, Christiansen B, Hardiman SC, Osprey SM, Yang S (2013) Multi-model analysis of Northern Hemisphere winter blocking: model biases and the role of resolution. J Geophys Res: Atmos 118:3956–3971. https://doi.org/10.1002/jgrd.50231

Ballinger TJ, Mote TL, Mattingly K, Bliss AC, Hanna E, van As D, Prieto M, Gharehchahi S, Fettweis X, Noël B, Smeets PCJP, Reijmer CH, Ribergaard MH, Cappelen J (2019) Greenland ice sheet late-season melt: investigating multiscale drivers of K-transect

events. Cryosphere 13:2241–2257. https://doi.org/10.5194/tc-13-2241-2019
Barrett BS, Henderson GR, McDonnell E, Henry M, Mote T (2020) Extreme Greenland blocking and high-latitude moisture transport. Atmos Sci Lett 21:e1002. https://doi.org/10.1002/asl.1002
Berckmans J, Woollings T, Demory M-E, Vidale P-L, Roberts M (2013) Atmospheric blocking in a high resolution climate model: influences of mean state, orography and eddy forcing. Atmos Sci Lett 14:34–40. https://doi.org/10.1002/asl2.412
Coles S, Bawa J, Trenner L, Dorazio P (2001) An introduction to statistical modeling of extreme values. Springer
Davini P, D'Andrea F (2016) Northern Hemisphere atmospheric blocking representation in global climate models: twenty years of improvements? J Clim 29:8823–8840. https://doi.org/10.1175/JCLI-D-16-0242.1
Davini P, D'Andrea F (2020) From CMIP3 to CMIP6: Northern Hemisphere atmospheric blocking simulation in present and future climate. J Clim 33:10021–10038. https://doi.org/10.1175/JCLI-D-19-0862.1
Davini P, Cagnazzo C, Gualdi S, Navarra A (2012) Bidimensional diagnostics, variability, and trends of Northern Hemisphere blocking. J Clim 25:6496–6509. https://doi.org/10.1175/JCLI-D-12-00032.1
Davini P, Corti S, D'Andrea F, Rivière G, von Hardenberg J (2017) Improved winter European atmospheric blocking frequencies in high-resolution global climate simulations. J Adv Model Earth Syst 9:2615–2634. https://doi.org/10.1002/2017MS001082
Dawson A, Palmer TN (2015) Simulating weather regimes: impact of model resolution and stochastic parameterization. Clim Dyn 44:2177–2193. https://doi.org/10.1007/s00382-014-2238-x
Delhasse A, Hanna E, Kittel C, Fettweis X (2021) Brief communication: CMIP6 does not suggest any atmospheric blocking increase in summer over Greenland by 2100. Int J Climatol 41:2589–2596. https://doi.org/10.1002/joc.6977
Elliott RD, Smith TB (1949) A study of the effects of large blocking highs on the general circulation in the northern-hemisphere westerlies. J Atmos Sci 6:68–85. https://doi.org/10.1175/1520-0469(1949)006%3c0068:ASOTEO%3e2.0.CO;2
Eyring V, Bony S, Meehl GA, Senior CA, Stevens B, Stouffer RJ, Taylor KE (2016) Overview of the coupled model intercomparison project phase 6 (CMIP6) experimental design and organization. Geosci Model Dev 9:1937–1958. https://doi.org/10.5194/gmd-9-1937-2016
Famooss Paolini L, Athanasiadis PJ, Ruggieri P, Bellucci A (2022) The atmospheric response to meridional shifts of the Gulf Stream SST front and its dependence on model resolution. J Clim 35:6007–6030. https://doi.org/10.1175/JCLI-D-21-0530.1
Fettweis X, Hanna E, Lang C, Belleflamme A, Erpicum M, Gallée H (2013) Brief communication "Important role of the mid-tropospheric atmospheric circulation in the recent surface melt increase over the Greenland ice sheet." Cryosphere 7:241–248. https://doi.org/10.5194/tc-7-241-2013
Gibson PB, Perkins-Kirkpatrick SE, Uotila P, Pepler AS, Alexander LV (2017) On the use of self-organizing maps for studying climate extremes. J Geophys Res: Atmos 122:3891–3903. https://doi.org/10.1002/2016JD026256
Greening K, Hodgson A (2019) Atmospheric analysis of the cold late February and early March 2018 over the UK. Weather 74:79–85. https://doi.org/10.1002/wea.3467
Haarsma RJ, Roberts MJ, Vidale PL, Senior CA, Bellucci A, Bao Q, Chang P, Corti S, Fučkar NS, Guemas V, von Hardenberg J, Hazeleger W, Kodama C, Koenigk T, Leung LR, Lu J, Luo JJ, Mao J, Mizielinski MS, Mizuta R, Nobre P, Satoh M, Scoccimarro E, Semmler T, Small J, von Storch JS (2016) High resolution model intercomparison project (HighResMIP v1.0) for CMIP6. Geosci Model Dev. 9:4185–4208. https://doi.org/10.5194/gmd-9-4185-2016
Hanna E, Cropper TE, Hall RJ, Cappelen J (2016) Greenland blocking index 1851–2015: a regional climate change signal. Int J Climatol 36:4847–4861. https://doi.org/10.1002/joc.4673
Hanna E, Hall RJ, Overland JE (2017) Can Arctic warming influence UK extreme weather? Weather 72:346–352. https://doi.org/10.1002/wea.2981
Hanna E, Fettweis X, Hall RJ (2018a) Brief communication: recent changes in summer Greenland blocking captured by none of the CMIP5 models. Cryosphere 12:3287–3292. https://doi.org/10.5194/tc-12-3287-2018
Hanna E, Hall RJ, Cropper TE, Ballinger TJ, Wake L, Mote T, Cappelen J (2018b) Greenland blocking index daily series 1851–2015: analysis of changes in extremes and links with North Atlantic and UK climate variability and change. Int J Climatol 38:3546–3564. https://doi.org/10.1002/joc.5516
Hanna E, Cappelen J, Fettweis X, Mernild SH, Mote TL, Mottram R, Steffen K, Ballinger TJ, Hall RJ (2021) Greenland surface air temperature changes from 1981 to 2019 and implications for ice-sheet melt and mass-balance change. Int J Climatol 41:E1336–E1352. https://doi.org/10.1002/joc.6771
Hanna E, Cropper TE, Hall RJ, Cornes RC, Barriendos M (2022) Extended North Atlantic oscillation and Greenland blocking indices 1800–2020 from new meteorological reanalysis. Atmosphere 13:436
Hauser S, Teubler F, Riemer M, Knippertz P, Grams CM (2024) Life cycle dynamics of Greenland blocking from a potential vorticity perspective. Weather Clim Dyn 5:633–658. https://doi.org/10.5194/wcd-5-633-2024
Hermann M, Papritz L, Wernli H (2020) A Lagrangian analysis of the dynamical and thermodynamic drivers of large-scale Greenland melt events during 1979–2017. Weather Clim Dyn 1:497–518. https://doi.org/10.5194/wcd-1-497-2020
Hersbach H, Bell B, Berrisford P, Hirahara S, Horányi A, Muñoz-Sabater J, Nicolas J, Peubey C, Radu R, Schepers D, Simmons A, Soci C, Abdalla S, Abellan X, Balsamo G, Bechtold P, Biavati G, Bidlot J, Bonavita M, De Chiara G, Dahlgren P, Dee D, Diamantakis M, Dragani R, Flemming J, Forbes R, Fuentes M, Geer A, Haimberger L, Healy S, Hogan RJ, Hólm E, Janisková M, Keeley S, Laloyaux P, Lopez P, Lupu C, Radnoti G, de Rosnay P, Rozum I, Vamborg F, Villaume S, Thépaut J-N (2020) The ERA5 global reanalysis. Q J R Meteorol Soc 146:1999–2049. https://doi.org/10.1002/qj.3803
Jury MW, Herrera S, Gutiérrez JM, Barriopedro D (2019) Blocking representation in the ERA-Interim driven EURO-CORDEX RCMs. Clim Dyn 52:3291–3306. https://doi.org/10.1007/s00382-018-4335-8
Kautz LA, Martius O, Pfahl S, Pinto JG, Ramos AM, Sousa PM, Woollings T (2022) Atmospheric blocking and weather extremes over the Euro-Atlantic sector – a review. Weather Clim Dyn 3:305–336. https://doi.org/10.5194/wcd-3-305-2022
Kohonen T (1990) The self-organizing map. Proc IEEE 78:1464–1480
Kohonen T (2013) Essentials of the self-organizing map. Neural Netw 37:52–65. https://doi.org/10.1016/j.neunet.2012.09.018
Lenggenhager S, Martius O (2019) Atmospheric blocks modulate the odds of heavy precipitation events in Europe. Clim Dyn 53:4155–4171. https://doi.org/10.1007/s00382-019-04779-0
Lennard C, Hegerl G (2015) Relating changes in synoptic circulation to the surface rainfall response using self-organising maps. Clim Dyn 44:861–879. https://doi.org/10.1007/s00382-014-2169-6
Lin G-F, Chen L-H (2006) Identification of homogeneous regions for regional frequency analysis using the self-organizing map. J Hydrol 324:1–9. https://doi.org/10.1016/j.jhydrol.2005.09.009
Liu Q (1994) On the definition and persistence of blocking. Tellus A 46:286–298. https://doi.org/10.1034/j.1600-0870.1994.t01-2-00004.x

Maddison JW, Gray SL, Martínez-Alvarado O, Williams KD (2019) Upstream cyclone influence on the predictability of block onsets over the Euro-Atlantic region. Mon Weather Rev 147:1277–1296. https://doi.org/10.1175/MWR-D-18-0226.1

Maddison JW, Gray SL, Martínez-Alvarado O, Williams KD (2020) Impact of model upgrades on diabatic processes in extratropical cyclones and downstream forecast evolution. Q J R Meteorol Soc 146:1322–1350. https://doi.org/10.1002/qj.3739

Maddison JW, Catto JL, Hanna E, Luu LN, Screen JA (2024) Missing increase in summer Greenland blocking in climate models. Geophys Res Lett 51:e2024GL108505. https://doi.org/10.1029/2024GL108505

Mathews J, Czaja A (2024) Oceanic maintenance of atmospheric blocking in wintertime in the North Atlantic. Clim Dyn. https://doi.org/10.1007/s00382-024-07196-0

Mattingly KS, McLeod JT, Knox JA, Shepherd JM, Mote TL (2015) A climatological assessment of Greenland blocking conditions associated with the track of Hurricane Sandy and historical North Atlantic hurricanes. Int J Climatol 35:746–760. https://doi.org/10.1002/joc.4018

Mattingly KS, Ramseyer CA, Rosen JJ, Mote TL, Muthyala R (2016) Increasing water vapor transport to the Greenland Ice Sheet revealed using self-organizing maps. Geophys Res Lett 43:9250–9258. https://doi.org/10.1002/2016GL070424

McLeod JT, Mote TL (2015) Assessing the role of precursor cyclones on the formation of extreme Greenland blocking episodes and their impact on summer melting across the Greenland ice sheet. J Geophys Res: Atmos 120:12357–12377. https://doi.org/10.1002/2015JD023945

Michel C, Rivière G, Terray L, Joly B (2012) The dynamical link between surface cyclones, upper-tropospheric Rossby wave breaking and the life cycle of the Scandinavian blocking. Geophys Res Lett. https://doi.org/10.1029/2012GL051682

Nakamura N, Huang CSY (2018) Atmospheric blocking as a traffic jam in the jet stream. Science 361:42–47. https://doi.org/10.1126/science.aat0721

Nghiem SV, Hall DK, Mote TL, Tedesco M, Albert MR, Keegan K, Shuman CA, DiGirolamo NE, Neumann G (2012) The extreme melt across the Greenland ice sheet in 2012. Geophys Res Lett. https://doi.org/10.1029/2012GL053611

Novak L, Ambaum MHP, Tailleux R (2015) The life cycle of the North Atlantic storm track. J Atmos Sci 72:821–833. https://doi.org/10.1175/JAS-D-14-0082.1

O'Reilly CH, Minobe S, Kuwano-Yoshida A (2016) The influence of the Gulf Stream on wintertime European blocking. Clim Dyn 47:1545–1567. https://doi.org/10.1007/s00382-015-2919-0

Odoulami RC, Wolski P, New M (2023) Attributing the driving mechanisms of the 2015–2017 drought in the Western Cape (South Africa) using self-organising maps. Environ Res Lett 18:074043

Ohba M, Kadokura S, Nohara D, Toyoda Y (2016) Rainfall downscaling of weekly ensemble forecasts using self-organising maps. Tellus a: Dyn Meteorol Oceanogr 68:29293. https://doi.org/10.3402/tellusa.v68.29293

Ossó A, Sutton R, Shaffrey L, Dong B (2018) Observational evidence of European summer weather patterns predictable from spring. Proc Natl Acad Sci 115:59–63. https://doi.org/10.1073/pnas.1713146114

Ossó A, Shaffrey L, Dong B, Sutton R (2019) Impact of air–sea coupling on Northern Hemisphere summer climate and the monsoon–desert teleconnection. Clim Dyn 53:5063–5078. https://doi.org/10.1007/s00382-019-04846-6

Overland JE, Francis JA, Hanna E, Wang M (2012) The recent shift in early summer Arctic atmospheric circulation. Geophys Res Lett. https://doi.org/10.1029/2012GL053268

Pasquier JT, Pfahl S, Grams CM (2019) Modulation of atmospheric river occurrence and associated precipitation extremes in the North Atlantic region by European weather regimes. Geophys Res Lett 46:1014–1023. https://doi.org/10.1029/2018GL081194

Pelly JL, Hoskins BJ (2003) A new perspective on blocking. J Atmos Sci 60:743–755. https://doi.org/10.1175/1520-0469(2003)060%3c0743:ANPOB%3e2.0.CO;2

Pettersen C, Henderson SA, Mattingly KS, Bennartz R, Breeden ML (2022) The critical role of Euro-Atlantic blocking in promoting snowfall in central Greenland. J Geophys Res Atmosp 127:e2021JD035776. https://doi.org/10.1029/2021JD035776

Pinheiro MC, Ullrich PA, Grotjahn R (2019) Atmospheric blocking and intercomparison of objective detection methods: flow field characteristics. Clim Dyn 53:4189–4216. https://doi.org/10.1007/s00382-019-04782-5

Preece JR, Wachowicz LJ, Mote TL, Tedesco M, Fettweis X (2022) Summer Greenland Blocking diversity and its impact on the surface mass balance of the Greenland ice sheet. J Geophys Res: Atmos 127:e2021JD035489. https://doi.org/10.1029/2021JD035489

Reusch DB, Alley RB, Hewitson BC (2005) Relative performance of self-organizing maps and principal component analysis in pattern extraction from synthetic climatological data. Polar Geogr 29:188–212. https://doi.org/10.1080/789610199

Rex DF (1950a) Blocking action in the middle troposphere and its effect upon regional climate. II. The climatology of blocking action. Tellus 2:275–301. https://doi.org/10.1111/j.2153-3490.1950.tb00339.x

Rex DF (1950b) Blocking action in the middle troposphere and its effect upon regional climate. I. An aerological study of blocking action. Tellus 2:196–211. https://doi.org/10.1111/j.2153-3490.1950.tb00331.x

Scaife AA, Woollings T, Knight J, Martin G, Hinton T (2010) Atmospheric blocking and mean biases in climate models. J Clim 23:6143–6152. https://doi.org/10.1175/2010JCLI3728.1

Scaife AA, Copsey D, Gordon C, Harris C, Hinton T, Keeley S, O'Neill A, Roberts M, Williams K (2011) Improved Atlantic winter blocking in a climate model. Geophys Res Lett. https://doi.org/10.1029/2011GL049573

Schiemann R, Demory M-E, Shaffrey LC, Strachan J, Vidale PL, Mizielinski MS, Roberts MJ, Matsueda M, Wehner MF, Jung T (2017) The resolution sensitivity of Northern Hemisphere Blocking in four 25-km atmospheric global circulation models. J Clim 30:337–358. https://doi.org/10.1175/JCLI-D-16-0100.1

Schiemann R, Athanasiadis P, Barriopedro D, Doblas-Reyes F, Lohmann K, Roberts MJ, Sein DV, Roberts CD, Terray L, Vidale PL (2020) Northern Hemisphere blocking simulation in current climate models: evaluating progress from the climate model intercomparison project phase 5 to 6 and sensitivity to resolution. Weather Clim Dynam 1:277–292. https://doi.org/10.5194/wcd-1-277-2020

Simonson JM, Birkel SD, Maasch KA, Mayewski PA, Lyon B, Carleton AM (2022) Association between recent U.S. northeast precipitation trends and Greenland blocking. Int J Climatol 42:5682–5693. https://doi.org/10.1002/joc.7555

Steinfeld D, Pfahl S (2019) The role of latent heating in atmospheric blocking dynamics: a global climatology. Clim Dyn 53:6159–6180. https://doi.org/10.1007/s00382-019-04919-6

Steinfeld D, Boettcher M, Forbes R, Pfahl S (2020) The sensitivity of atmospheric blocking to upstream latent heating – numerical experiments. Weather Clim Dyn 1:405–426. https://doi.org/10.5194/wcd-1-405-2020

Von Storch H, Zwiers FW (2002) Statistical analysis in climate research, Cambridge university press

Wachowicz LJ, Preece JR, Mote TL, Barrett BS, Henderson GR (2021) Historical trends of seasonal Greenland blocking under different

blocking metrics. Int J Climatol 41:E3263–E3278. https://doi.org/10.1002/joc.6923

Wang H, Luo D (2022) North Atlantic footprint of summer Greenland ice sheet melting on interannual to interdecadal time scales: a Greenland blocking perspective. J Clim 35:1939–1961. https://doi.org/10.1175/JCLI-D-21-0382.1

Wang S, Nath D, Chen W, Wang L (2019) Recent strengthening of Greenland blocking drives summertime surface warming over Northern Canada and Eastern Siberia. J Clim 32:3263–3278. https://doi.org/10.1175/JCLI-D-18-0410.1

Ward JL, Flanner MG, Dunn-Sigouin E (2020) Impacts of Greenland block location on clouds and surface energy fluxes over the Greenland ice sheet. J Geophys Res: Atmos 125:e2020JD033172. https://doi.org/10.1029/2020JD033172

Wazneh H, Gachon P, Laprise R, de Vernal A, Tremblay B (2021) Atmospheric blocking events in the North Atlantic: trends and links to climate anomalies and teleconnections. Clim Dyn 56:2199–2221. https://doi.org/10.1007/s00382-020-05583-x

Wills SM, Thompson DWJ, Ciasto LM (2016) On the observed relationships between variability in gulf stream sea surface temperatures and the atmospheric circulation over the North Atlantic. J Clim 29:3719–3730. https://doi.org/10.1175/JCLI-D-15-0820.1

Woollings T, Barriopedro D, Methven J, Son S-W, Martius O, Harvey B, Sillmann J, Lupo AR, Seneviratne S (2018) Blocking and its response to climate change. Curr Clim Chang Rep 4:287–300. https://doi.org/10.1007/s40641-018-0108-z

Yamamoto A, Nonaka M, Martineau P, Yamazaki A, Kwon YO, Nakamura H, Taguchi B (2021) Oceanic moisture sources contributing to wintertime Euro-Atlantic blocking. Weather Clim Dyn 2:819–840. https://doi.org/10.5194/wcd-2-819-2021

Yao Y, De-Hai L (2014) The anomalous European climates linked to different Euro-Atlantic blocking. Atmos Oceanic Sci Lett 7:309–313. https://doi.org/10.3878/j.issn.1674-2834.14.0001